ISAS - INTERNATIONAL SCHOOL FOR ADVANCED STUDIES

Far-Ultraviolet Energy Distribution of OB stars and the UVSTAR mission

Thesis presented by
Miguel Chavez Dagostino
for the degree of
"Magister Philosophiae"

Supervisor: Prof. Roberto Stalio
Astrophysycs sector
SISSA/ISAS
Academic year 1992/1993

TRIESTE

SISSA - SCUOLA INTERNAZIONALE SUPERIORE DI STUDI AVANZATI
TRIESTE
Strada Costiera 11

Table of Contents

0 Introduction

Although several space missions have pushed the observation of hot stars up to the Lyman limit and beyond -(Ultraviolet Spectrometers on board the *Voyagers* 1 and 2, Broadfoot *et al.* (1977), sounding rockets; Woods, Feldman and Brune (1985); Brune, Mount and Feldman, (1979); Carruthers *et al.* (1981); Cook, Cash and Snow (1989), and very recently the Astro-1 mission on board the Shuttle Columbia, Davidsen *et al.* (1992))-, the spectral region in the 912-1250$\AA$ band is still poorly observed and the number of studied stars is very reduced. This spectral region was also explored by the *Copernicus* satellite, but due to problems with the instrument stability, the spectra from *Copernicus* are not calibrated.

The study of hot stars in the Far-Ultraviolet, FUV, is very important for a number of reasons. First of all they emit most of their radiation in the FUV and therefore it is natural to look for signatures in this band. The spectral energy distribution (SED) of this type of stars is affected by numerous physical processes, such as line and wind-blanketing and the poorly characterized interstellar extinction below 1200 $\AA$. Secondly, because of their great luminosity stars of spectral types O and B possess radiation-pressure driven winds as indicated by the P-Cygni profiles of the UV resonant lines of abundant ions. Finally, the FUV band provides potential discriminants and diagnostics for shock structures in the outflowing winds.

As introductory remarks I will summarize some of the most important problems to the analysis of winds in OB stars and mention the useful insights to be given by the quatitative analysis of observations at the wavelengths non-accessible to International Ultraviolet Explorer (*IUE*) satellite or the Hubble Space Telescope (*HST*). For the spectral band above

Lyman α there have been published excellent reviews regarding the contribution of *IUE* to the understanding of the physics involed in the photosperes and winds of early-type stars (see for example Snow and Stalio 1987, Howarth and Wilson 1991).

0.1 Galactic O and B stars

- Ionization fractions. Together with the *IUE* spectra, access to the wavelength range below 1200 $\AA$ will allow to observe the ionization balance between different stages of several elements. Particularly important for understanding the ionization conditions in photospheres and envelopes will be the detection of resonance and excited lines from the wind, such as C III(977), O VI(1032,1038), P V(1118,1128) S IV(1063,1073), C III*(1176) and N IV*(955).

- Determination of $\dot{M}$ from a larger range of ionization. The quantitative interpretation of the considered best indicators of mass-loss accessible to *IUE* usually represent a difficult task. The lines are either saturated or they represent minor ionization fractions. Observations below 1200 $\AA$ will permit to analyse non-saturated features of less abundant elements (than C, N and O) such as Sulphur and Phosphorus and features arising from the major ionization stages, avoiding in this way the uncertainties introduced when correcting the ionization fractions.

- Terminal velocity from ions that have a maximun ionization fraction. FUV data from will provide more accurate terminal velocities (to about 10 %) and determine the influence of the ionization conditions on the values of v_∞ obtained analysing *IUE* high resolution spectra (*e.g.* Groenewegen *et al.* 1989).

- Superionized circumstellar material in B and B*e* stars. The presence of extended blue wings in the UV resonance lines -down to B2 V in Normal B stars and to B9.5 IV in B*e* stars- is unclear (Marlborough and Peters 1982). It is thought that different mechanisms of ionization operate in B and B*e*stars and that perhaps these mechanisms

give rise to the Be properties in B stars. Very useful insights for understanding the Be phenomenon will be obtained if extend the observations for a larger range of ions. The location of formation of different ion spices would provide information of the geometry and physical conditions of the circumstellar regions evidenced by optical and UV observations. Matching the observations in a wide range of wavelenghts -FUV, UV, optical and IR- theoretical models for the envelopes may lead to unmask the possible relationships among the peculiarities found in Be stars and perhaps to map these peculiarities along the Be-B-Be cycle.

0.2 Magellanic cloud stars

- Effects of Chemical abundance in the wind. Results from *IUE* suggest that the ionization conditions in SMC stars are the same than those found in the galactic counterparts (Prinja 1987) indicating that the mass-loss rates are equal. This in turn contradicts the radiation driven wind theories which predict a decrement of the mass-loss rate with decreasing metallicity. The analysis of the intensity ratios between different ionization stages in the FUV for different elements would allow to establish the differences in ionization conditions and the corresponding ones in mass-loss rates.

0.3 Interstellar material

- Characterization of the extinction curve down to the lyman limit. Extinction curves below the *IUE* cutoff have been derived using data from *Copernicus* and *Voyager* UVS. With higher resolution than that provided by *Voyager* it will be possible to derive directly from observations, instead from models, the significant contribution of molecular hydrogen to extinction.

- Measurements of the column density of HI and H_2. Quantitative analysis of the Lyman (1108$\AA$) and Werner (1009$\AA$) bands of H_2 and features of HI will permit direct determination of the column densities of this material along different lines of sight.

Therefore, apart from giving knowledge about the very important contribution of the gas to the interstellar absorption, it will be possible to map the distribution of this material around the sun.

0.4 Goals of this work

Almost any observation with enhanced sensitivity and resolution with respect to previous observations has great potential of discovery. Among the future space projects carrying FUV sensitive instrumentation is the *UVSTAR* experiment described in the chapter 1. The main goal of the present thesis is to compare the spectral energy distribution of a selected sample of main-sequence OB stars observed by *IUE* with the predictions of models atmospheres. This comparison will serve as an starting point towards creating a stellar data base that will contain all potential FUV sources within its detection capabilities. The procedires and results of this comparison are explaines in chapter 2. In chapter 2 we briefly describe the current status of observations of OB stars shortward of Ly α. In this same chapter we present the results of comparing model atmodpheres predictions with the sensitivity of *UVSTAR* and derived the limiting magnitudes of stars of different spectral types accessible to *UVSTAR*. The effect of the interstellar reddening on exposure times is also estimated.

1 The UVSTAR Experiment

UVSTAR, UltraViolet Spectrographic Telescope for Astronomical Research, is a spectrographic telescope for observations of astronomical and planetary sources; it operates in the 500-1250 $\AA$ wavelength band at 1$\AA$ resolution. The experiment has capability for long slit spectral imaging of extended cosmic sources such as planets, planetary nebulae, supernova remnants, H II regions, and external galaxies. *UVSTAR* will fly as a Hitchhiker-M payload on the Shuttle (Fig. 1.1) and will be part of the IEH (International EUV/FUV Hitchhiker) mission. The first of the 5 flights approved by NASA is expected to take place early in 1995.

UVSTAR consists of a movable platform and an optical system. The platform will provide fine pointing ($\pm$ 5 arcsec) within 3° from the nominal view direction, which is near the Shuttle +Y axis, i.e. perpendicular to the long axis of the Shuttle and in the plane of the wings. The optical system consists of a set of two telescopes and Rowland concave-grating spectrographs with intensified CCD detectors. The first spectrograph telescope (FUV) operates in the 850-1250 $\AA$ spectral range; the second (EUV) covers the 500-900 $\AA$ region. A number of pointed observations will be made of calibration targets, planets, ultraviolet stellar sources and extended objects. At any time the *UVSTAR* is pointed toward the hemisphere outward from the Earth and the Shuttle is on celestial lock, it is possible that a source of interest for UV astronomy will be within the pointing range. In this case, *UVSTAR* will operate in a "serendipitous/target-of-opportunity" mode; in this mode targets that will have been defined in advanced will be acquired and observed. *UVSTAR* will carry out some 25$\pm$ 5 "pointed" observations flight. A similar number of pointed observations will be available to

the planetary physics program. At the end of the program we will have observed 100 to 150 astronomy sources. About half of them will be 1)calibration, 2) EUV, and 3) extended sources.

1.1 Technical Description

UVSTAR has two nearly identical spectrograph channels (EUV and FUV) that will observe simultaneously the same target. Each channel consists of a telescope mirror and a concave grating spectrograph with its own intensified CCD detector. The telescope form images of the target at the entrance slit of the spectrographs. The concave gratings of the spectrographs both disperse and re-image the light from the target onto the 2-D detectors. Spatial resolution along the slit is preserved, so that in the cross-dispersion direction the detectors record many spectra corresponding to different parts of the source simultaneously. The optical design is driven by the fact that at the EUV wavelengths of interest

- only reflective optics can be used
- reflectivities are poor, which requires minimizing the number of reflections if weak sources are to be detected in a short period of time

1.2 The Telescopes

The telescopes mirrors are off-axis paraboloids of 30 cm of diameter and 1.5 m focal length. They are SiC coated for maximum reflectivity; are made of Zerodur to prevent defocusing due to thermal changes; are joined to the spectrographs by rods of carbon composite material of about zero thermal expansion coefficient along its length.

1.3 The Spectrographs

Each spectrograph employs a single concave, holographic to disperse the radiation and focus it on the detector. Holographically ruled gratings can achieve aberration correction and

flat focal plane over a length of 8mm in the cross-dispersion and 15.4 mm in the dispersion directions. The 70×100mm gratings have a radius of curvature of 275mm. To maintain good focus over a range of temperatures, the gratings will be fabricated on Zerodur blanks. The grating cell is mounted to permit small motions relative to the spectrograph housing. The position of the grating relative to the entrance slit and detector is established by invar rods that extend from the grating cell to fixed positions near the entrance slit and detector.

The two spectrographs cover the overlapping spectral ranges, 500-900 $\AA$ and 850-1250 $\AA$. In each case the spectrum of about 400 $\AA$ is dispersed along 1152 pixels, giving a dispersion of 0.35 $\AA$/pixel. The array is 298 pixels wide. In the image mode the spectral/spatial images are comprised of 2×1152×298 pixels, that is nearly 7×10^5 pixels or 1.4×10^6 bytes if each pixel is digitized to a 16-bit accuracy. The read out format is controlled by computer so that it can be matched to the needs of a particular experiment.

Each of the spectrographs is equipped with mechanism for selecting among three entrance slits. All slits have the same length of 0.25 deg but differ in width. The slits widths and their uses are:

- Narrow slit (3 pixels, 9 arcsec). This slit will provide 1 $\AA$ resolution.
- Medium slit (13 pixels, 39 arcsec). This slit will give global images of extended sources (PN, SN Remnants) at the wavelengths of the most intense emissions. Resolution is 4.5 $\AA$.
- Wide slit (33 pixels, 100 arcsec). This aperture will allow the whole image if the Io plasma torus (for details of the planetary program see Stalio *et al.* 1992) to be dispersed into its major emissions and re-imaged with a resolution of 12 $\AA$.

1.4 Detectors

The intensified CCD (ICCD) detectors consist of standard proximity-focused image intensifier tubes that are fiber-optically coupled to CCDs. They have successfully flown in previous

missions. Both image intensifiers are windowless. Charge from photoevents is amplified by the microchannel plate and electrostatically accelarated to a phosphor screen on a fiberoptic window. The visible-wavelength image from the phospor is transferred to the CCD by fiber optics for readout. A special position of the slit changning mechanisms seals the spectrograph enclosures to protect the detectors and grating from contamination. Each spectrograph is equipped with a small ion pump to provide a satisfactory vacuum environment for operating the windowless intensifiers on orbit.

1.5 Sensitivity

The ICCD detectors of *UVSTAR* are 2-D detectors with photon-counting capability. The overall instrument performance is related to the rate at which photoevents are generated at the photocathode of the detector. For the imaging spectrographs, Table 1.1 gives the sensitivity for two kinds of source, namely a a point source of continuum emission and an extended source of monochromatic emission. The wavelengths are in $\mathring{A}$, the area of the telescope mirror (A) is in cm^2 , Ω is the solid angle measured in sr, corresponding to the field of a single pixel, δ ($\mathring{A}$/pixel) is the spectral dispersion, σ is the reflective-dispersive efficiency of the grating, ϵ is the quantum efficiency of the photocathode, μ is the reflective efficiency of the telescope, R is the response for a point source in units counts/pixel/s per photon/cm /s/$\mathring{A}$, S is the response for monocromatic emission of brigtness I Rayleighs; the units are counts/pixel/s per Rayleigh.

1.6 Guiding and other characteristics

UVSTAR includes capabilities for independent target acquisition and tracking. The spectrograph package has internal gimbals that allow angular movement of $\pm 3^o$ from the central position. Rotation about the azimuth axis (parallel to the Shuttle Z axis) and elevation axis (parallel to the Shuttle X axis) will actively position the field of view (FOV) to center the target of interest in the fields of the spectrographs.

Two dedicated visible imagers (Finder and Tracker) having different fields of view and a quadrature diode, provide guiding information. The finder has 60 mm focal length and f/1.4 optics giving a FOV of 6^0 x 8^0. The system works in two modes: Finder mode: From a coarse knowledge of the pointing direction ($\pm 3^0$), the system recognizes autonomously the acquired stellar field and point to the chosen direction within ± 5". Tracker mode: After having reached the wanted direction, it operates with three different techniques: 1)same as the finder mode:at every acquisition, the system repeats the star field identification routine. In this mode the algorithm requires, on average, a processing time of 300 ms (on a 386/387 at 25 MHz). 2) Triangulation mode: the system chooses three stars out of the stars selected in the finder mode and by means of a triangulation procedure, calculates the position of the center of the sensor which concides with the chosen pointing direction. In this case the algorithm needs a few ms of processing time. 3) Star pointing mode: the target star is at the center of the sensor. We correct its position at every acquisition keeping it at the center. The algorithm takes only few ms of processing time.

As an alternative to the above mentioned routines we have developed procedure (planet mode) which does not use any indentification procedure, but simply searches for the brightest object in the FOV, brings it at the sensor center and tracks with the algorithm 3.

The tracker is a 75 mm diameter cassagrain telescope with a focal length of 1.5 m and a FOV of $0.24^0 \times 0.32^0$. Finder and Tracker have their own ICCD detector, 384×288 pixel arrays. The tracker ICCD will have the same plate spectrograph. In addition the tracker telescope will also be equipped with an intensified quadrature diode which will track a 8-9 magnitude star with negligible processing time. The diameter of the photodiode is 3 mm and the star image will be 1 mm. The tracking accuracy will be better than ±5".

2 SED of OB stars (1200-1900 $\mathring{A}$)

We present the comparison between the observed 1200-1900 $\mathring{A}$ fluxes of more than 100 early type stars and those predicted by the most recent classical LTE, line-blanketed models of Kurucz. High quality *IUE* spectra from *ULDA (Uniform Low Dispersion Archive)* are selected. The average of the observed fluxes for each spectral class calculated in three narrow bands centered at 1300, 1500 and 1750 $\mathring{A}$ is compared with model atmosphere calculation using different T_{eff} scales found in the literature. We found that, at the wavelengths considered, models and observational data are in agreement within the observational uncertainties. It should be mention however, that the observed energy distributions are sistematically steeper than the computed ones as indicated by the FUV colors. We confirm the small dependence of the UV fluxes (normalized to the visual flux) on temperature for the stars with spectral types earlier than B1.

Determination of photospheric parameters through the comparison between the observed and computed SED has been extensively studied (Morossi and Malgnini 1985; Longo *et al.* 1989, hereafter LSPR). In the wavelength region longward 1200$\mathring{A}$ the agreement in the 10 % level is virtually universal. The purpose of the work developed in the present chapter is to establish a set of models that best fit the *IUE* data and use this models to predict absolute fluxes at wavelengths below the *IUE* cutoff. The analysis has been carried out in a somewhat similar way as Papaj *et al.* (1991).

2.1 Data analysis

In the following, we describe the sample of selected stars, the correction for extinction and give comments about some of the objects.

2.1.1 Description of the sample

O Stars: From *ULDA* data base we extracted 65 spectra of O stars. Only stars observed with the Short Wave Prime, large aperture and for which the spectra have high quality exposure code were selected. We then excluded from this sample the members of the Magellanic Clouds, those stars which in the *SIMBAD* data base are not classified as O stars and the subdwarf O stars. The sample was arbitrarily divided into three groups; O5 and earlier, O6-O7 and O8-O9. More the half of the O stars are luminosity class V. Several objects that show variability were also included as well as some objects with emission lines and/or peculiar spectrum.

The final sample of O stars and their basic parameters are listed in Table 2.1. Columns (1)-(7) list the image number of the selected *ULDA* spectra, the HD or BD number of the star, the star name, the visual magnutide, B-V, the color excess (calculated from the observed colors and the intrinsic color indices listed in Schmidt-Kaler (1982)) and spectral type. V, B-V and spectral type were taken from *SIMBAD* data base. For some stars there was not UVB information in *SIMBAD*; in this case we have used different sources (listed in notes to Table 2.1) for the color excess and spectral type.

B stars: As well as in O stars the spectra of B stars are those obtained with the SWP and large aperture. The exposure code for all of them corresponds to high quality spectra. We selected from the original sample of 230 stars only the stars with luminosity class V. In our sample there is only one star classified as peculiar, HD 64740. The final list is shown in Table 2.2. The contents specification is as Table 2.1. Again the V, B-V and the spectral types are from *SIMBAD*. A few stars have variability measurements reported in *SIMBAD* and this is indicated in notes to Table 2.2.

A stars: We have included in our analysis a small group of A stars. The information provided in Table 2.3 comes from the same sources as before.

2.1.2 Correction for extinction

It has been widely investigated whether it really exists a general extinction law for the ultraviolet region or if the presence of anomalous curves is indeed a more common phenomenon. Several authors have carried out extensive work on producing mean extinction curves finding out that, with the exception of a few individual stars, the departures from a fixed curve are not significant (Nandy *et al.* 1975, 1976) whereas others (eg. Carnochan, 1986 and Thé *et al.*, 1989) have obtained very striking results indicating that for up to one half of the stars the received radiation may be affected by anomalous extinction in either or both the 2200 Å feature and the so-called FUV rise.

In calculating the intrinsic fluxes we took into account that some objects lie in regions with anomalous extinction. For O stars, most of which have color excesses (E_{B-V}) larger than 0.20, we corrected the spectra for interstellar extinction using the the extinction curves in Aiello *et al.* (1988). For HD 168076 we used the value of R_V =3.9 reported by Thé *et al.* (1990). For the members of the Carina Nebula region we estimated the values of R_V from the color excess diagram E(B-V) vs E(V-I) in Herbst (1976), taking into account that for R_V =3.1 and 5, E(V-I)/E(B-V) is 1.62 and 2.58 respectivelly. For the star HD 93250 we used the curve given in Aiello's *et al.* paper.

For B stars no attemp was made before hand to detect stars with anomalous extinction, instead we corrected all the spectra using the the mean extinction curve of Mathis (1990, R_V =3.1) and then looked for possible peculiarities in those stars whose spectra were well apart from the main group of spectra in each spectral subclass. Some of the B stars resulted affected by anomalous extinction in part or the whole spectral region analized in the present work. The spectra of these stars were corrected with the Aiello's *et al.* extinction curves when available. B stars with anomalous extinction reported in the literature, but non included in

Aiello's *et al.* sample were omitted from the calculations. The groups of A stars were corrected with Mathis' curve for R_V =3.1

In Figs. 2.1 and 2.2 we show the spectra of our program stars corrected for extinction as described above and normalized to the visual magnitude. Also these figures show the mean spectrum for each spectral class and the 2σ dispersion (dashed lines).

For the A1-A3 stars illustrated in Fig. 2.3 no attempt was made to obtain the mean flux distribution because the drop in the energy distribution varies greatly below 1400Å.

2.1.3 Comments on individual stars

After inspection of Figs. 2.1 the following stars appear to be peculiar in the sense that their spectra was either above or bellow the group of spectra of the rest of the stars in each spectral class:

HD 54669 is the only star for which the UBV photometry does not match with the spectral type. *SIMBAD* reports B-V=-0.20 and spectral type B4 V. However, for such a spectral type the intrinsic color index is -0.18. Garrison *et al.* (1977) classified HD 54669 as a B2 V. We have used this spectral type to determine its color excess.

HD 154445 and HD 329729 have abnormal extinction (Carnochan 1986 and Aiello *et al.* 1988. We used the curves given by the later authors to deredden the spectra of these stars.

HD 152560 might be missclassified or its spectrum contaminated by an early-type companion. According to Roundtree and Sonnenborn (1991) the CIV (1550Å) line should be absent in stars of spectral types B2 and later. In Fig. 2.1 we see that this line is strong in this star while absent in the rest of B2 stars.

HD 211880 and HD 21428. Carnochan (1986) reports anomalous extinction for both stars, but Aiello *et al.* did not include them in their sample.

2.2 Model Atmospheres

The assumptions made in contructing the classical models fail when dealing with hot (T_{eff} > 30000K) or low gravity stars. Several authors have discussed the validity of using LTE models for these hottest stars. Torres (1987) found that the predictions from LTE models fit better the observed energy distribution than those obtained using NLTE models suggesting the line blanketing effects are more important than NLTE effects. Also, the effects of the strong stellar winds on the flux distribution turn out to be of the small according to Hummer (1982) and Abbott and Hummer (1985).

LSPR presented low dispersion spectra of 20 OB stars observed with the *Voyager 1* and *Voyager 2* UV spectrometers and with the *IUE* and *TD-1* satellites. They compared their data with the Kurucz models (Code ATLAS8) and concluded that the models represent a valid method to predict the energy distribution in OB stars (even in the hottest stars in their sample where the NLTE effects are expected to be important), but they are not useful for determining fundamental stellar quantities, T_{eff} and Log g because of the slight dependence of the flux on these parameters.

We have used the Code ATLAS9 to compute models for each spectral class from O8 to A0. For B stars the values of the input parameters required by the models were taken from Underhill (1982) (Log g) and Schmidt-Kaler (1982) (T_{eff}). For O and A stars both parameters were taken from Schmidt-Kaler (1982). The temperature for spectral class B4 was obtained by interpolation. Since we are dealing with disk population stars, we used only solar abundances. The effects of the abundance and gravity are small longward to the Lyman limit and become more important at shorter wavelengths (Mihalas 1978). In all models we have used v_{turb} = 2km/s. The resolution of the computed spectra is approximately 10Å between 912 and 1900Å. Among the improvements of ATLAS9 relevant to the present work, is a larger number of atomic transitions than previous codes and new opacity distribution functions.

2.3 Observed vs. Computed fluxes

In Figs. 2.4 *a* and *b* we plot together the observed mean normalized fluxes for the groups of B and A stars, and the flux distributions from the models. In Fig. 2.4 *a* the top four of the observed spectra appear to be more tightened because the mean spectral distributions for B0.5 and B1.5 stars have been included. In the same figure the fact that the spectra for B3 and B4 stars overlap is certainly due to selection effects in our sample.

The comparison was made by averaging the normalized fluxes for each spectral subclass in three narrow bands (50$\AA$ width) centered at 1300, 1500 and 1750 $\AA$. In Table 2.4 we tabulate the mean fluxes, one σ dispersion and the resulting fluxes from the models. Models and observations agreed within 10 % for B3 stars and earlier. For later types the observed flux distribution exceed by up to a factor of 2 model predictions. In order to explain these sistematic differences we explored several posibilities. The use of a shallower extinction curve such as that of Seaton (1979) would decrease the absolute level of the observed fluxes. Mathis' and Seaton's standard curves differ by up to 0.52 magnitudes at 1300 $\AA$ which correspond to a difference in logarithmic fluxes of Log F_S−log F_M =0.20(E_{B-V}). Since most of the stars in our sample have color excesses less than 0.10 we do not expect large corrections in our fluxes, in fact we estimated the correction of the order of 0.01 in the normalized fluxes with the exception of B4 stars where the correction is 0.03. Hence using Seatos's curve cannot account for the observed differences.

Another possibility that gave us positive results was the use of other T_{eff} scales to run the models. This in fact was expected since the flux level strongly depends on effective temperature for stars in the temperature range 10000-25000K. In Fig. 2.5 the comparison between the observed (filled squares) and computed fluxes (dashed lines) is illustrated. The three different dashed lines correspond to the model results obtained by using the T_{eff}-spectral-type relationship of Bohm-Vitense (1981), Schmidt-Kaler (1982) and Theodossiou and Danezis (1991). The vertical error bars correspond to $\pm\sigma$ and the horizontal error

bars correspond to one spectral class uncertainty. For the three groups of O stars we have calculated a temperature from the weighed mean of the individual temperatures of the groups members. In the first two groups of O stars (empty squares in Fig. 2.5) we have not included error bars for the following reasons. First, because these stars are heavily reddened and the dispersion obtained in the averaging processes might be meaningless, and second, because we did not calculate models to compare the observed energy distribution of these stars.

The agreement between the models and *IUE* data is clear from Fig. 2.5. These results confirm previous ones (LSPR; Torres 1987) in the sense that the models appear to reproduce reasonably well the spectral energy distribution in early type stars. It should be mentioned however, that at 1300 *Å* *IUE* data is located sistematically above the results from the models independently of the effective temperature scale. The effect is more obvious whel looking at the slope of the energy distribution displayed in Fig. 2.6. This effect is in contrast to the results obtained by Malagnini *et al.* (1983) who found that the UV data from the S2/68 catalogue (Jamar *et al.* 1976) are smaller that the prediction of models with the largest differences at the shortest wavelengths (1360*Å*).

Although we did not compare the observations of the earlier O-type stars with models, it is interesting to note that the mean fluxes for these stars are not significantly different to the mean flux of B0 stars, moreover, two of the groups of O stars; O5 and O8-O9 are, in average, fainter than the rest of O and B0 stars. This behaviour was noticed by Massa and Savage (1985) when they compared the intrinsic fluxes of a sample of O stars with a reference B0 star, υ Ori.

2.4 Sources of error

To account for the dispersion shown in the averaged fluxes and possible errors in the mean values given in the previous section, we consider three main sources of error; photometric measurements V and B-V, the color excess E_{B-V} and the extinction law.

Since we have used the V magnitudes obtained by the several sources listed in *SIMBAD*

to normalize the FUV fluxes we assume an error (due to uncertanties in its determination and variability) of ± 0.05mag. This is an exagerated quotation; a more realistic value would be half of it. However, the influence of the uncertainty in V is small because the magnitude is an additive constant in the calculation of logarithmic fluxes. More important, however, is the color excess since it modifies both the shape and the absolute level of the flux distribution. Following the procedure of Thé *et al.* (1989) the error in the fluxes in given approximately by

$$\Delta F_\lambda / F_\lambda \approx 0.9 \Delta m_\lambda$$

If we consider an error of one spectral class in the intrinsic color indexes adopted in this work, the error on the E_{B-V} can be as large as 0.02 for O-type stars and 0.05 for B and A stars. This last uncertainty would lead to an error of the order of 40 % in the flux at 1300$\AA$ (equivalet to 0.20 in the logarithm of the normalized fluxes). Notice that the error in the flux depends on a factor giving the selective to visual extinction (A_λ / A_V) and therefore the error increases towards shorter wavelengths.

Another source of error is the sistematic use of a stardard extinction law to correct the stellar spectra. The effects of the correct choice of R_V is extremely important if the stars studied are heavily reddened (as most of our program O stars). The use of a standard extinction curve in HD 93205 would lead to an error in the normalized flux of the order of 0.53 at 1300$\AA$, twice as large as the error introduced by the uncertainties in spectral classification.

3 The 912-1250 $\mathring{A}$ band

3.1 3.1 Current status of observations below 1200$\mathring{A}$

The establishment of a reliable scale for the determination of absolute stellar fluxes at FUV wavelengths, in the region between 1200$\mathring{A}$ and the Lyman limit at 912$\mathring{A}$, has proved to be specially difficult. Independent determinations based, for the most part, on observations of brigth, luminous O and B stars have frequently led to widely divergent results. This differences have manifested themselves as absolute fluxes for the same star which may differ by factors as large as 4 to 6 at some wavelengths. This is in sharp contrast to the results obtained by several authors and the ones shown in the previous chapter at the wavelength region longward 1200$\mathring{A}$. So far the stellar calibration standards shortward to the Lyman limit refer to few rocket flights and *Voyager* observations (see references in the introduction). Large discrepancies have been found below 1200$\mathring{A}$ among the observations themselves and between the observations and model predictions. The spectrophotometric data obtained by the rocket groups is substantially lower than the predictions of the theoretical models while *Voyager* data are above by factors 1.5 to 2 of model predictions. Holberg *et al.* (1982) compared *Voyager* results with the available rocket data dividing the 912-1200$\mathring{A}$ spectral interval into three bands. The summary of his comparison is the following. At 1200$\mathring{A}$ all the results agree within 10 %. In the 1050-1150$\mathring{A}$ interval *Voyager* fluxes are above the models by factors of 1.5-2.0 while the fluxes of Brune *et al.* (1979) are approxiamtely 20-60 % fainter than model predictions. Carruthers *et al.* (1981) fluxes are in good agreement with model predictions

down to 1050Å. Below 1050Å the largest discrepancies appear, the fluxes of *Voyager* remain above the theoretical models while Brune *et al.* (1979) data remain below. The fluxes of Carruthers (1981) fall drastically well below the models.

More recently Cook *et al.* (1989) used a sensitive rocket-borne spectrometer to obtain a 960-1270Å spectrum of Spica (α Vir). Again, the comparison of various results; *Voyager*, *IUE*, Brune *et al.* (1979) and theirs are in good agreement above 1200Å, and discrepancies arise below 1150Å.

In Fig. 3.1 we illustrate the comparison between *Voyager* (from LSPR) and theoretical FUV colors calculated using the T_{eff} that best fit *IUE* data in chapter 2. The intrinsic color indices are the average of the deredened fluxes in two bands at 950-1150 and 1300-1500 Å. *Voyager* data are sistematically above models predictions by up to factors of 2 (in absolute units). This difference seems to increase towards later spectral types reaching a factor of 7 at spectral type B5. It is not clear why such discrepancies exist. Holberg *et al.* (1991) conducted a detailed analysis of two hot subluminous stars, BD $+28^0$ 4211 a sdO and G191-B2B, a hot DA white dwarf. For these two cases they found that a single power law and a pure hydrogen model atmosphere provide an excellent match to the entire absolute energy distribution from 912 Å to 1 μm respectively. Among the possible explanations for the dramatic decrease of the stellar fluxes, accepting that these fluxes are "true", is the existence of a previously unrecognized source of opacity in the atmospheres of luminous O and B stars as was first invoked by Cook *et al.* (1989). On the other side, if we accept *Voyager* fluxes, it implies that rocket results are severly affected by either or both uncertainties in the calibration or a possible inflight contamination in some of these experiments (see discussion in Holberg *et al.* 1982.). The discrepancies with models atmospheres remain an open question. Additional photometric studies and detailed non-LTE (including line-blanketing) calculations are needed.

3.2 3.2 Predictions for *UVSTAR*

In this section we compare the expected sensitivity for *UVSTAR* with the predictions of model atmospheres and give an estimation of the exposure times for early-type stars.

For a point source of continuous emission having flux of Φ photons cm^{-2} s^{-1} $\AA^{-1}$ the sensitivity R is given by

$$R = \Phi A \sigma \epsilon \mu s [\text{Photoevents } s^{-1} \; pixel^{-1}]$$

The meaning of the above parameters was given in chapter 1. The threshold of detection and the errors depend only on the statistics. Assuming Poisson statistics one would require at least x^2 events in order to obtain measurements with a signal to noise ratio (S/N) of x. The measured flux is thus given by

$$F_\lambda = x^2 / R_\lambda t$$

where t is the exposure time in seconds and R_λ is the response derived for a unitary flux in erg cm^{-2} s^{-1} $\AA^{-1}$.

In chapter 2 we obtained the normalized fluxes $\log(F_\lambda/F_V)$. This quantity for each spectral type is to be the same outside the earth atmosphere for stars with little or no reddening. The expected flux outside the earth atmosphere in erg cm^{-2} s^{-1} $\AA^{-1}$, is given by

$$F_\lambda = 10^{(\Phi_s - 0.4V - 8.43)}$$

where we have used the relation $V = -2.5\log(F_V) - 21.017$ and we have defined $\Phi_s = \log(F_\lambda/F_V)$.

For reddened stars the flux F_λ should be multiplied by a factor corresponding to the correction for reddening in the visual magnitude and the FUV flux, hence in general one can write

$$F_\lambda = \alpha 10^{(\Phi_s - 0.4(V - R_V E_{B-V}) - 8.43 + 0.4[A_\lambda/A_V] R_V E_{B-V})}$$

The parameter α is included to account for the fraction of the stellar flux absorbed by molecular hydrogen if $\lambda < 1100$ $\AA$ where the Lyman series of H_2 begin. An estimation of this parameter has been reported by LSPR and Snow *et al.* (1990).

By using the set of relationships described above for λ =1050$\AA$ we have produced Fig. 3.2. The filled dots connected by dashed lines correspond to unreddened stars of the same visual magnitude and different spectral type. The vertical dashed line shows the expected limiting exposure time due to orbital contraints. The effects of reddening can be seen in Fig. 3.3. For this figure we have considered 25 minutes of integration time and a S/N=6. We should mention that by decreasing the resolution to about 6 $\AA$ (as that of *IUE*) one gain a bit less that two magnitudes.

4 Concluding remarks

We presented the comparison between the observed far ultraviolet fluxes for

nearly 120 stars in the range 1200-1900$\mathring{A}$. We confirmed the results obtained by several authors that the flux distribution in early type stars is adequately represented by the predictions of line-blanketed LTE models, though some discrepancies are apparent at the shortest wavelenths. O-type stars do not show significantly different FUV absolute fluxes of those of B0-type stars confirming previous results.

In view of the large observational discrepancies found so far in the 912-1200$\mathring{A}$ band and the lack of reliable standard calibration stars, the theoretical FUV fluxes were used to predict the observation capabilities of UVSTAR. We have created a catalogue containing nearly 35000 stars brighter than the limiting mignitudes (for unreddened stars) expected for UVSTAR. Certainly this number will be dramatically reduced once the effect of the interstellar extinction is taken into account.

References

Abbott, D. C., and Hummer, D. G., 1985, Ap.J., **294**, 286.

Aiello *et al.*, 1988, Astr.Ap.Suppl., **73**, 195.

Bohm-Vitense, E. 1981, Ann. Rev. Astron. Astrphys., **19**, 295.

Broadfoot *et al.* 1977, Space Sci. Rew., **21**, 183.

Brune, W. H., Mount, G. H., and Feldman, P. D., 1979, Ap.J., **227**, 884.

Carnochan, D. J., 1986, M.N.R.A.S., **219**, 903.

Carruthers, G. R., Heckathorn, H. M., and Opal, C. B., 1981, Ap.J., **243**, 855.

Cook T. A., Cash, W., and Snow T. P., 1989, Ap.J., **347**, L81-L84.

Conti, P. S., and Leep, E. M., 1974, Ap.J., **173**, 113.

Davidsen *et al.* 1992, Ap.J., **392**,264.

Garrison, R. F., Hiltner, W. A., and Schild, R. E., 1977, Ap.J.Suppl. **35** 111.

Groenewegen, M.A.T., Lamers, H. J. G. L. M., and Paulgrach, A. W. A., 1989, Astr.Ap., **221**, 78.

Herbst, W., 1976, Ap.J., **208**, 923.

Holberg, J. B., Forrester, W. T., Shemansky, D. E., and Barry, D. C., 1982, Ap.J., **257**, 656.

Howarth, I., and Wilson, R., 1991, Adv.Spa.Res, **11**, No.11, 15.

Hummer, D. G., 1982, Ap.J.,**257**, 724.

Jamar *et al.* Ultraviolet brigth spectrom.catal., ESA, SR-27.

Kurucz, R. L., 1979, Ap.J. Suppl. **40**,1.

Lesh, J. R., 1968, Ap.J.Suppl., **16**, 371.

Longo *et al.*, 1989, Ap.J., **339**, 474 (LSPR).

Malagnini, M. L.,Faraggiana, R., and Morossi, C., 1983, **128**, 375.

Marlborough, J. M. and Peters, G. J., 1982, in M. Jashek and H. -G. Groth (eds), *IAU Symp.* **98**, 361.

Morossi, C, and Malagnini, M. L., 1985, Astr.Ap.Suppl., **60**, 365.

Massa, D., and Savage, B. D., 1985, Ap.J. **299**, 305.

Mathis, J, S., 1990, Ann.Rev.Astron.Astrophys.,**28**, 37.

Mihalas, D., 1978, *Stellar Atmospheres*, W.H. Freeman & Co., San Francisco., 2nd. Edition.

Nandy *et al.* 1975, Astr.Ap., **44**, 195.

Nandy *et al.* 1976, Astr.Ap., **51**, 63.

Papaj, E., Wegner, W. and Krelowski, J., 1990, M.N.R.A.S., **246**, 408.

Prinja, R. K., 1987, M.N.R.A.S., **228**, 173.

Seaton , M. J., 1979, M.N.R.A.S., **187**, 73.

Schmidt-Kaler, Th., 1982, Landolt Börntein Catalogue, VI/2b.

Snow, T. P., and Witt, A., 1989, Ap.J., **342**, 295.

Snow, T. P., Allen, M. M., and Polidan, R. S., 1990, Ap.J.,**359** , L23-L27.

Thé *et al.*, 1989, Astr.Ap.Suppl., **81**, 115.

Thé *et al.*, 1990, Astr.Ap.Suppl., **82**, 319.

Theodossoiu, E. and Danezis, E., 1991, Ap. Spa. Sci., **183**, 91.

Torres, A. V., 1987, Ap.J., **322**, 949.

Underhill, A. B., 1982, *B stars with and without emission lines*, NASA-CNRS monograph series, Eds. A.B. Underhill and V. Doazan. NASA SP-456.

Walborn, N. R., 1973, A.J., **78**,1067.

Whittet, D. C. B., and van Breda, I G., 1980, M.N.R.A.S., **192**, 467.

Woods, T. N., Feldman, P. D., and Brune, G. H. 1985, Ap.J.,**292**, 676.

Figure captions

chapter 1

Fig 1.1 Sketch of the opto-mechanical configuration of UVSTAR.

chapter 2

Fig 2.1 Dereddened spectra of the program stars. For some the stars indicated in the boxes see text. The solid line represent the average spectrum shifted 1.2 vertical units. Dashed lines correspond to $\pm 2\sigma$ dispersion. The B7 star HD 87901 is well below the rest of B7 stars. We believe that since this star is very brigth, the spectrum is saturated

Fig 2.2 Same as **Fig 2.1** but averaged spectra is displayed in its correct units.

Fig 2.3 Dereddened spectra of A1-A3 stars. These groups of stars were not taken into account in our comparison because the amount of energy emitted in the FUV is very small. Only nearby stars will be observable below 1200$\AA$. Stars with enhanced metallicity will be even more difficult to observe since line blanketing greatly affects the flux level shortward of Lyα (Kurucz 1979).

Fig 2.4 a) Sequence of average dereddened spectra. For the sake of clarity we have omitted the spectra of O stars. b) Energy distributions from model atmospheres (T_{eff} from Schmidt-Kaler, 1982).

Fig 2.5 Comparison between the observed (filled squares) and computed (dashed lines)

fluxes normalized to the visual magnitude as a function of the spectral-type. The shortest dashed lines correspond to the computed models using T_{eff} from Schmidt-Kaler, 1982. The middle-size and longest dashed lines correspond to models computed with T_{eff} from Bohm-Vitense (1981) and Theodossiou and Danezis (1991) respectivelly. The empty squares indicate the fluxes derived for O stars.

Fig 2.6 Computed and observed FUV color indices vs spectral type.

chapter 3

Fig 3.1 Far ultraviolet colors and intrinsic color index relationship for some early-type stars. The filled squares represent the values given in LSPR for the main sequence and giants stars in their sample. The dots connected by a dashed line correspond to model predictions. It appears that the disagreement between *Voyager* data and model predictions increases towards later spectral types.

Fig. 3.2 *UVSTAR* sensitivity calculations for a S/N of 10 compared to model atmospheres predictions at λ =1050$\mathring{A}$. The vertical dashed line indicates the maximum integration time permitted by the orbital constraints.

Fig. 3.3 The diagram shows the limiting magnitude reachable for a S/N=6 at 1050$\mathring{A}$ and full resolution for different spectral types and different E(B-V). The effect of molecular hydrogen is also included.

Fig. 1.1

UVSTAR (UltraViolet Spectrographic Telescope for Astronomical Research)

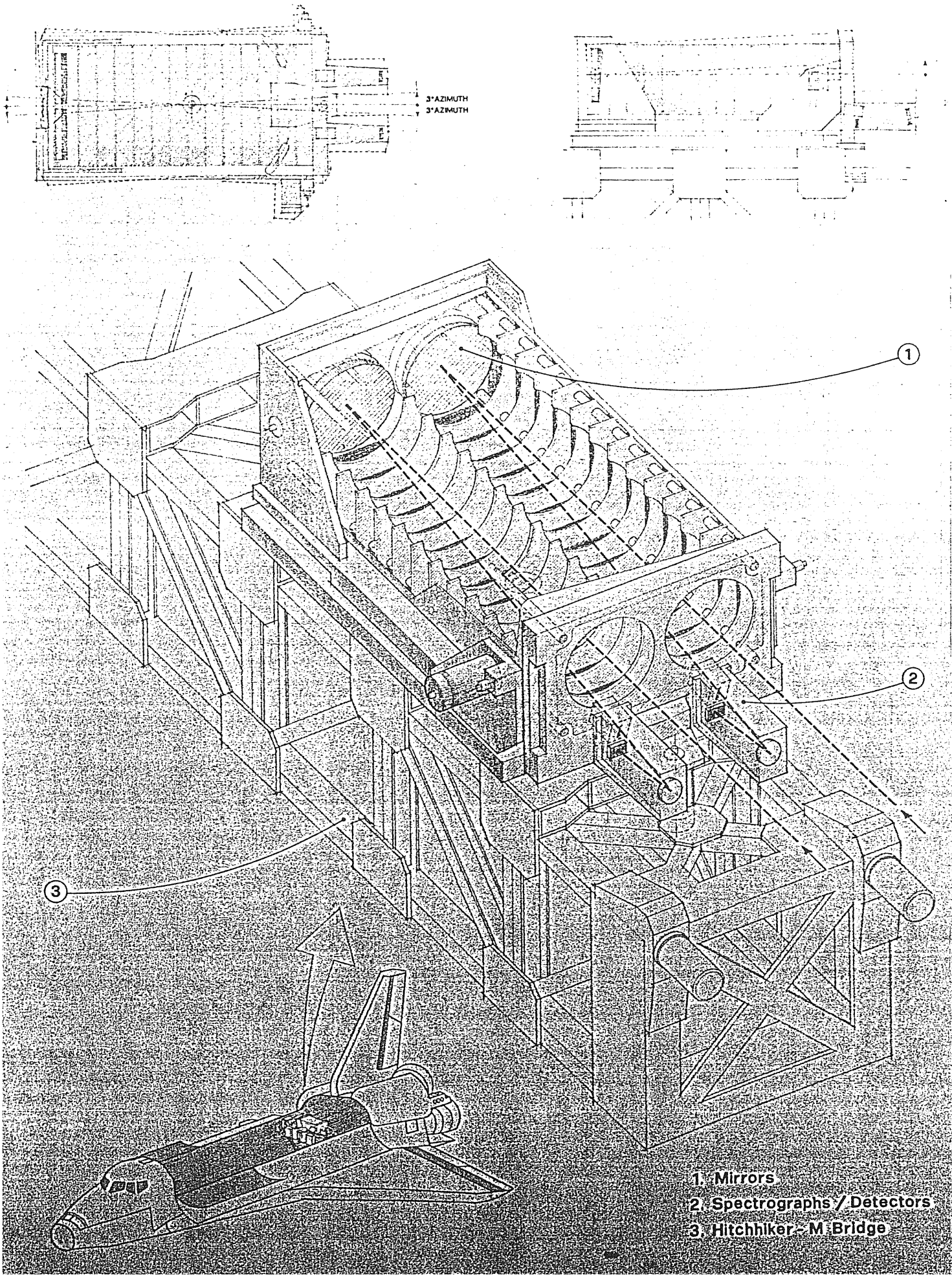

Fig. 2.1

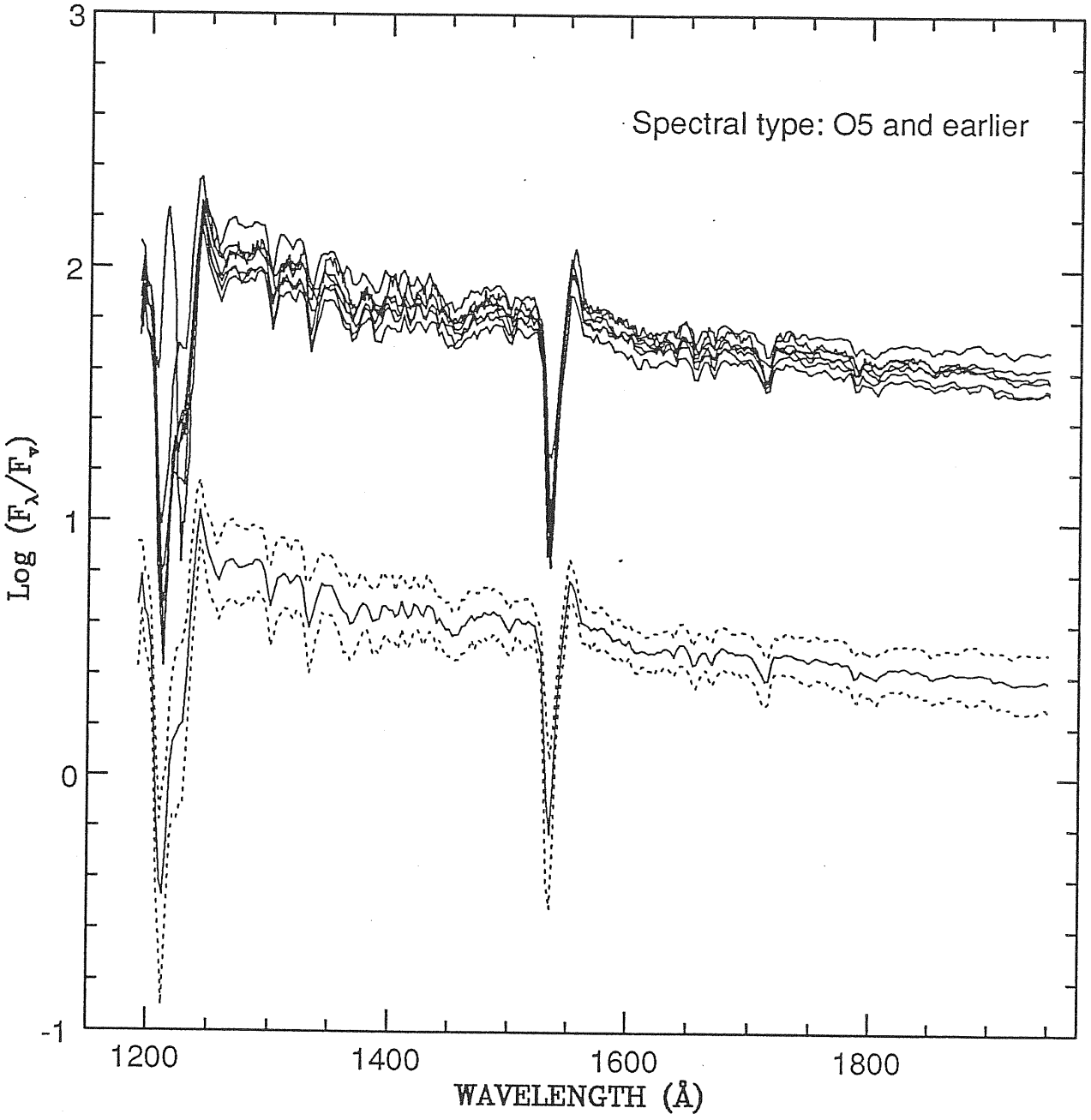
Spectral type: O5 and earlier
Log (F_λ/F_v)
3
2
1
0
-1
1200
1400
1600
1800
WAVELENGTH (Å)

Fig. 2.1 (continued)

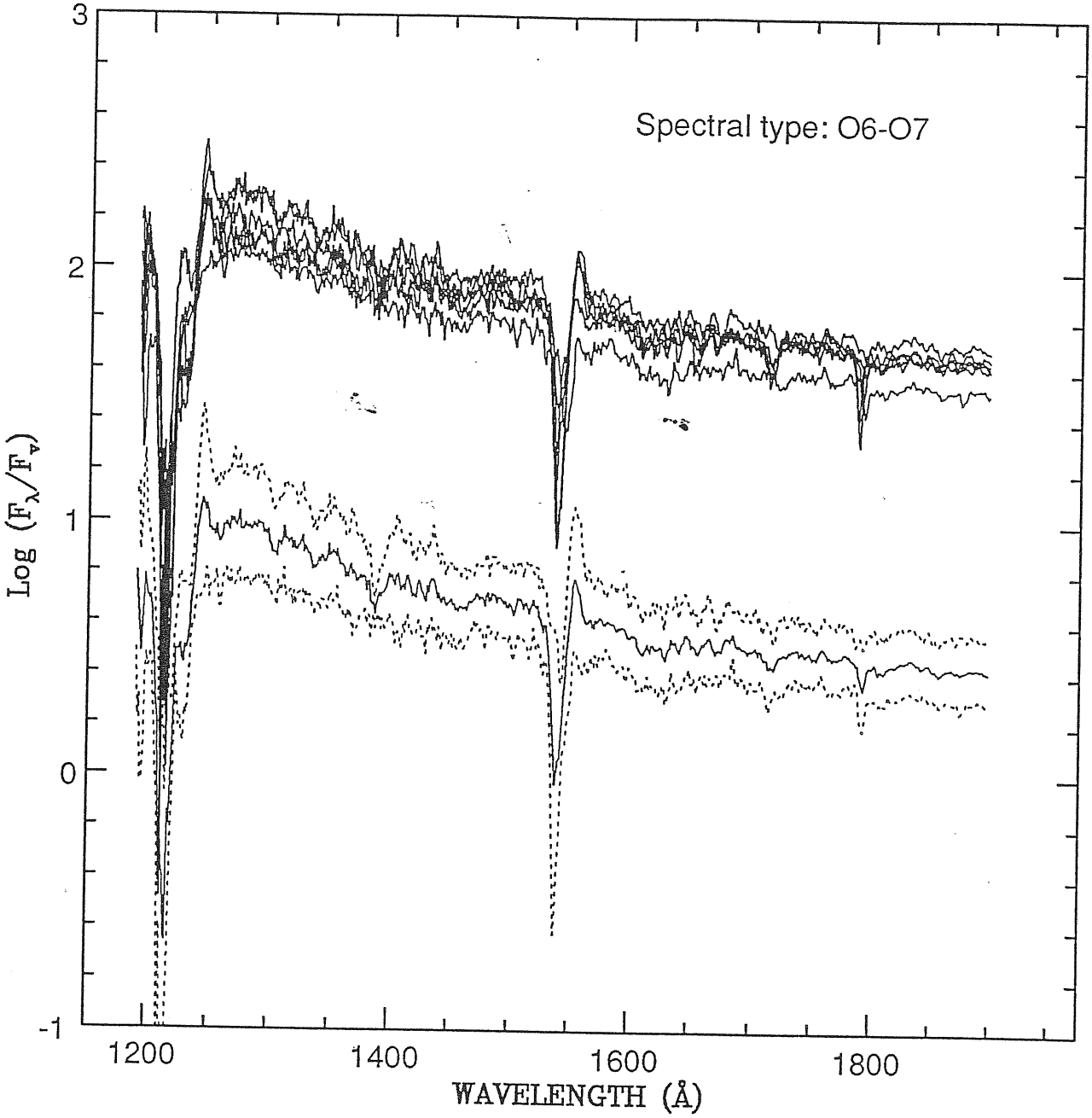

Fig. 2.1 (continued)

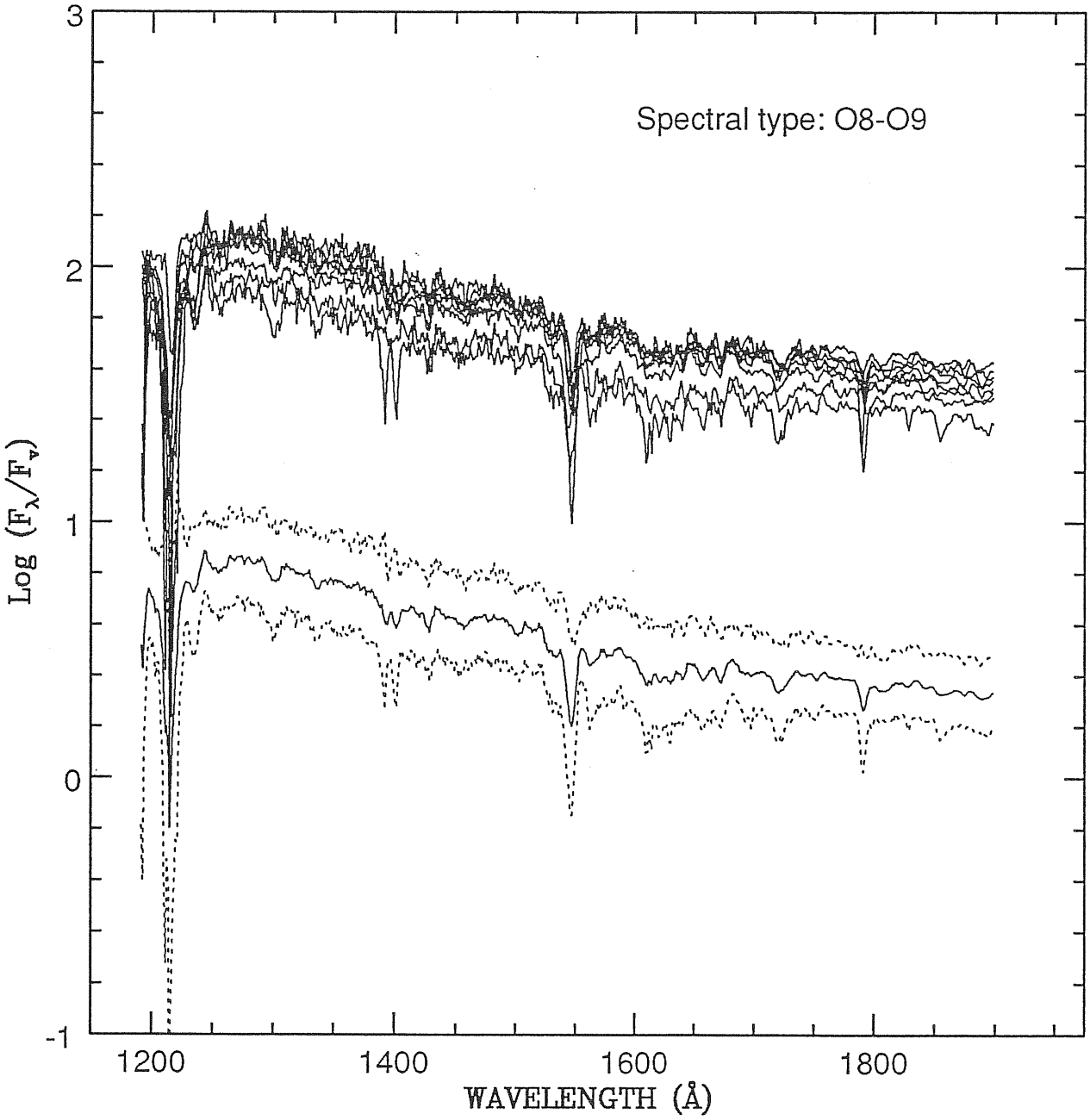

Fig. 2.1 (continued)

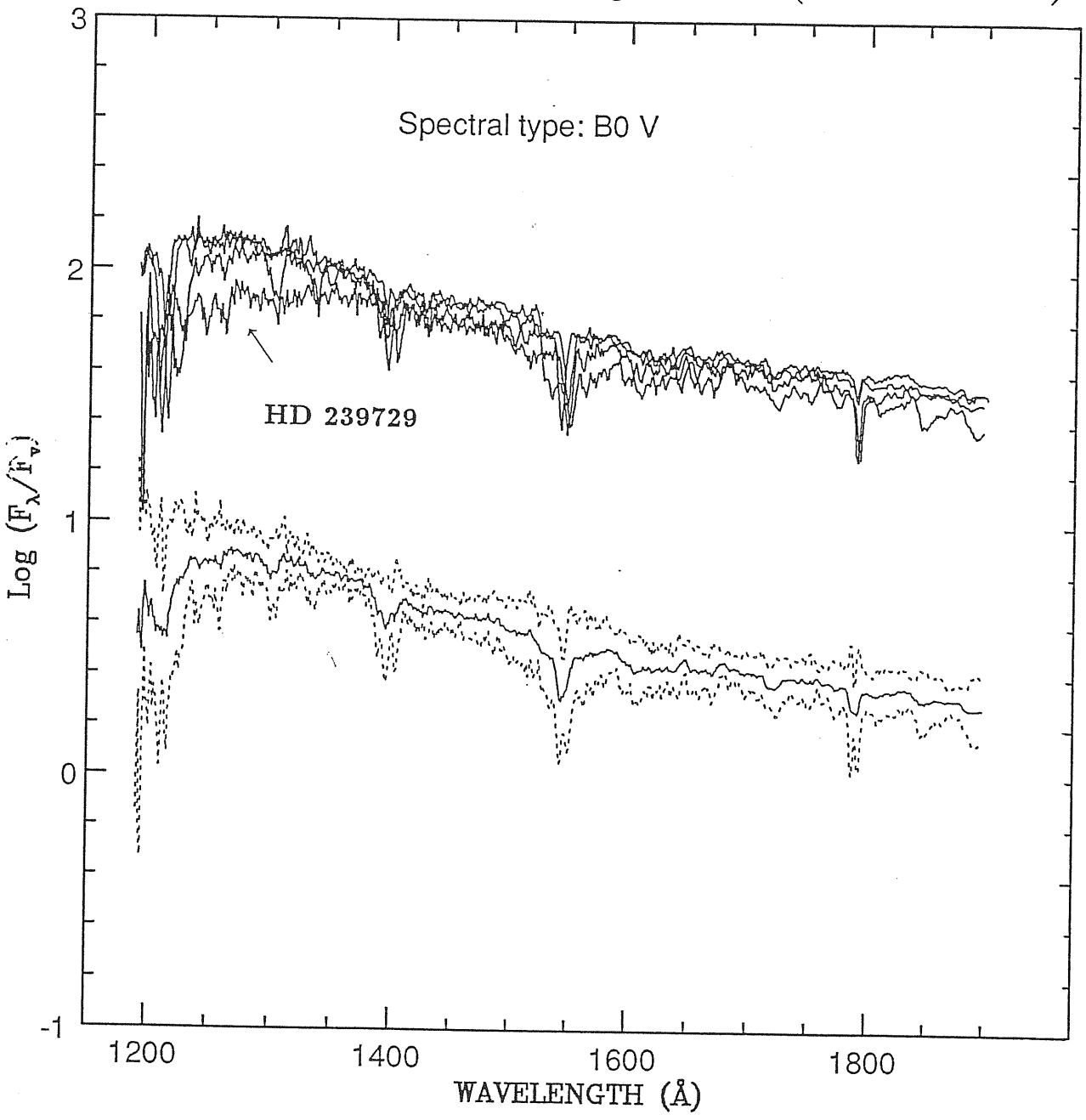

Fig. 2.1 (continued)

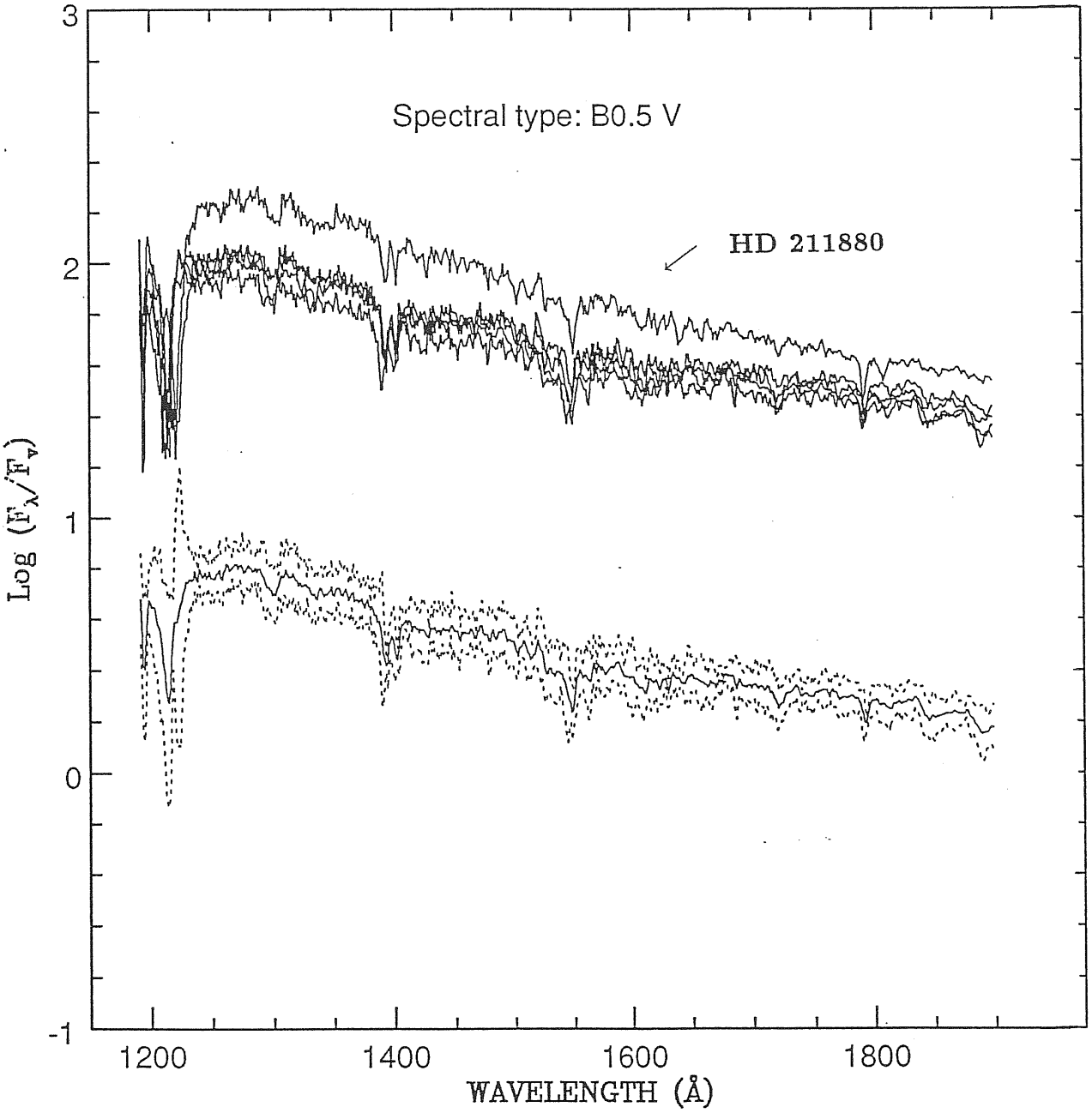

Fig. 2.1 (continued)

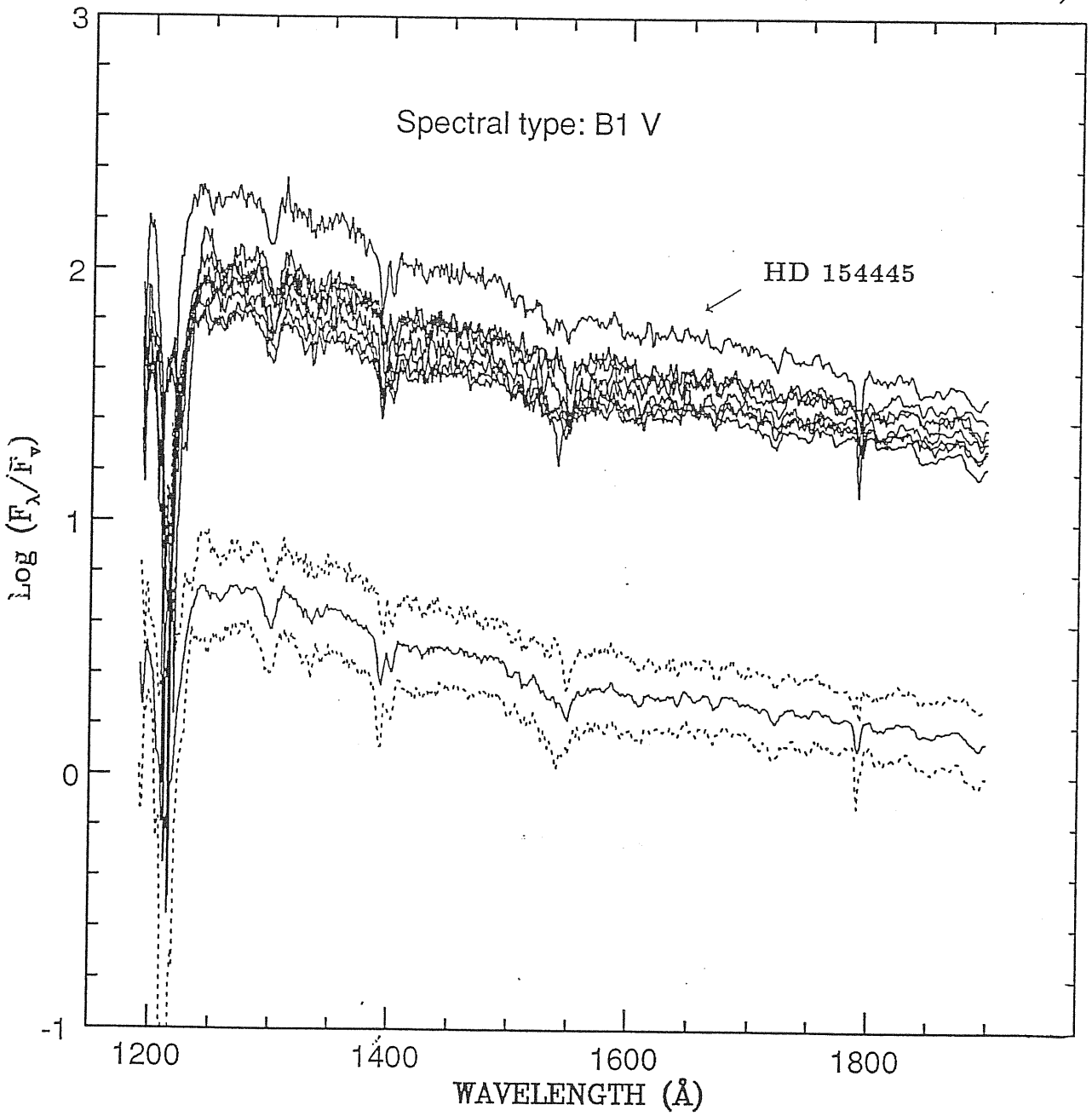

Fig. 2.1 (continued)

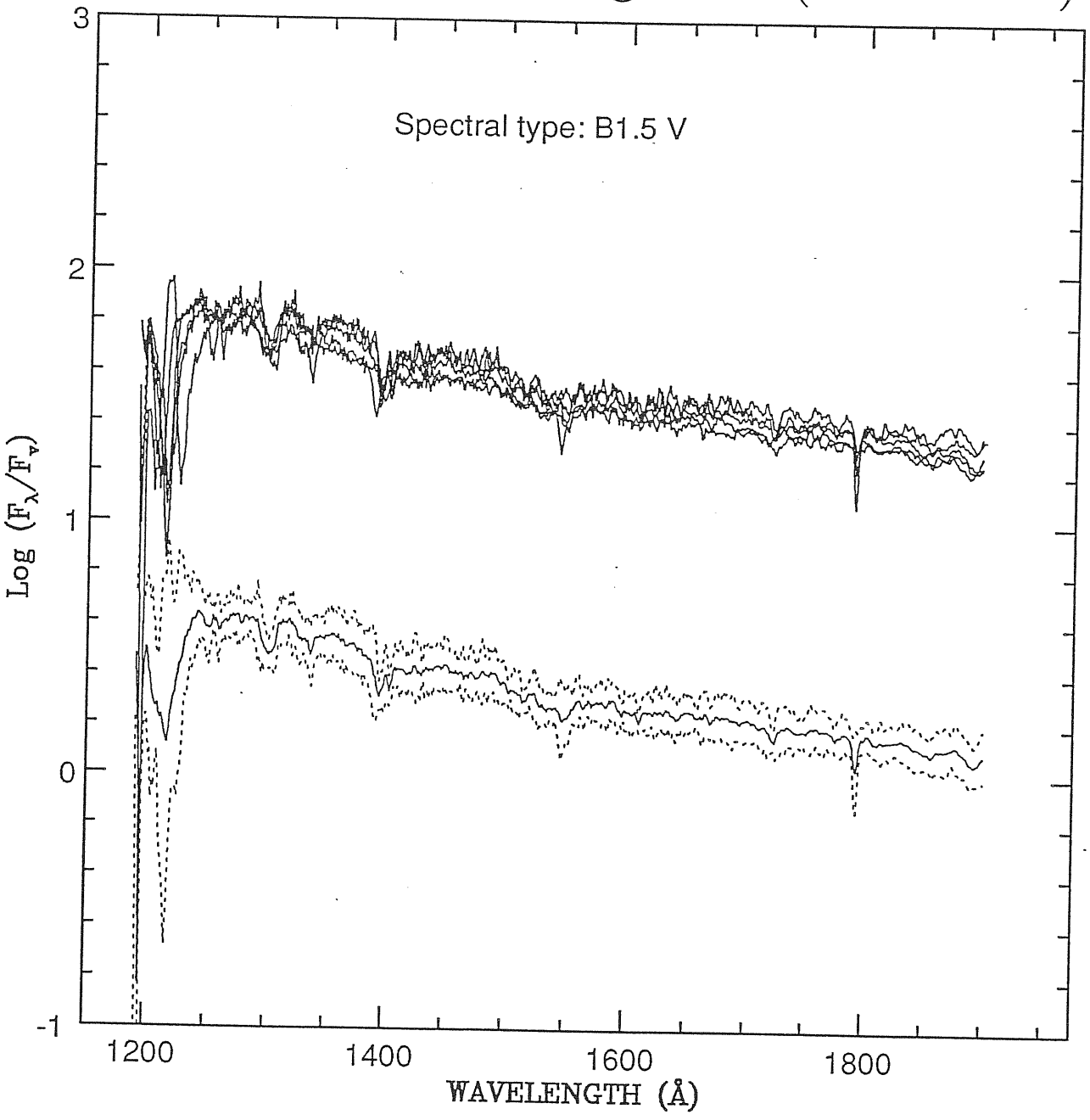

Fig. 2.1 (continued)

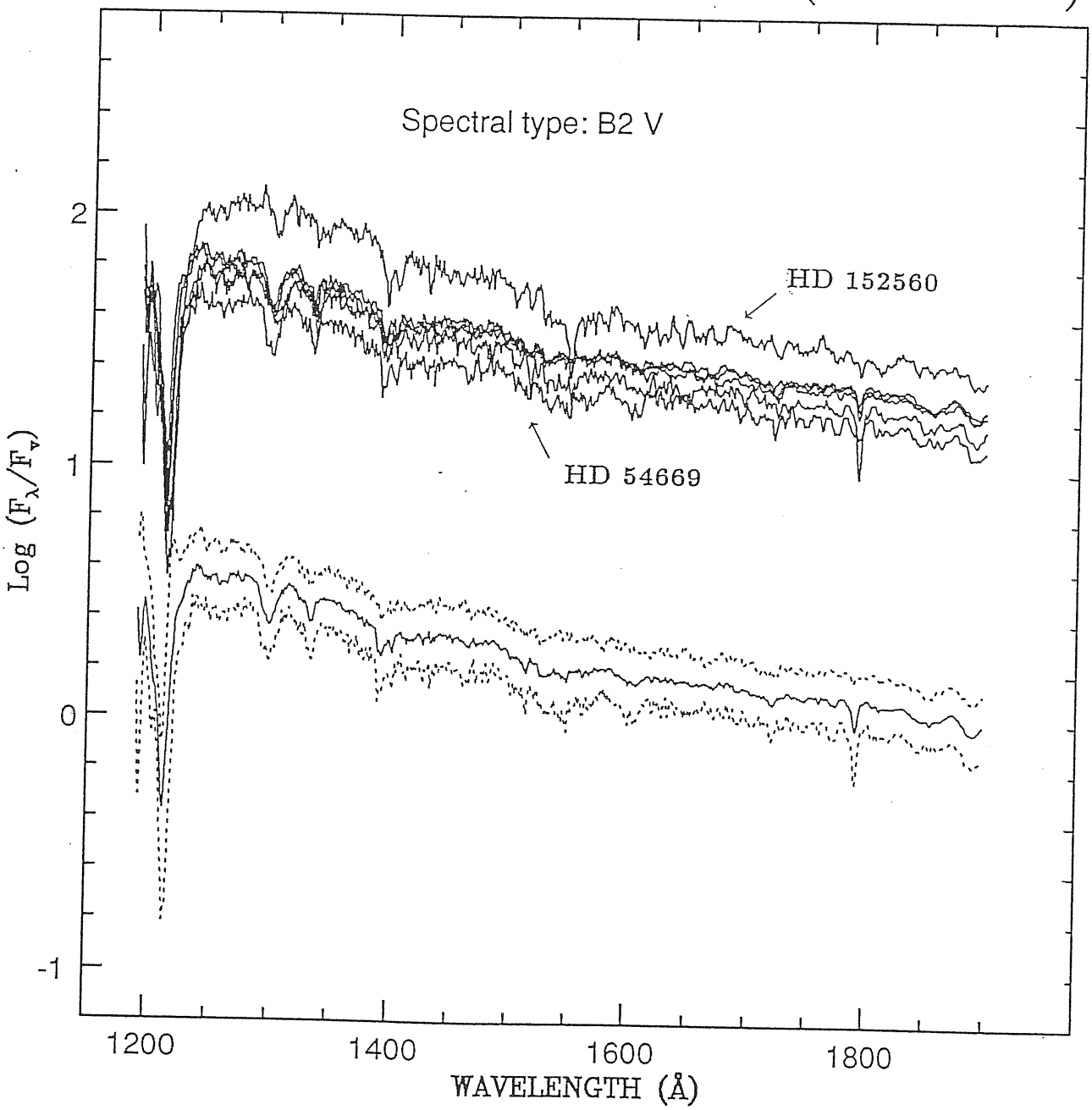

Fig. 2.1 (continued)

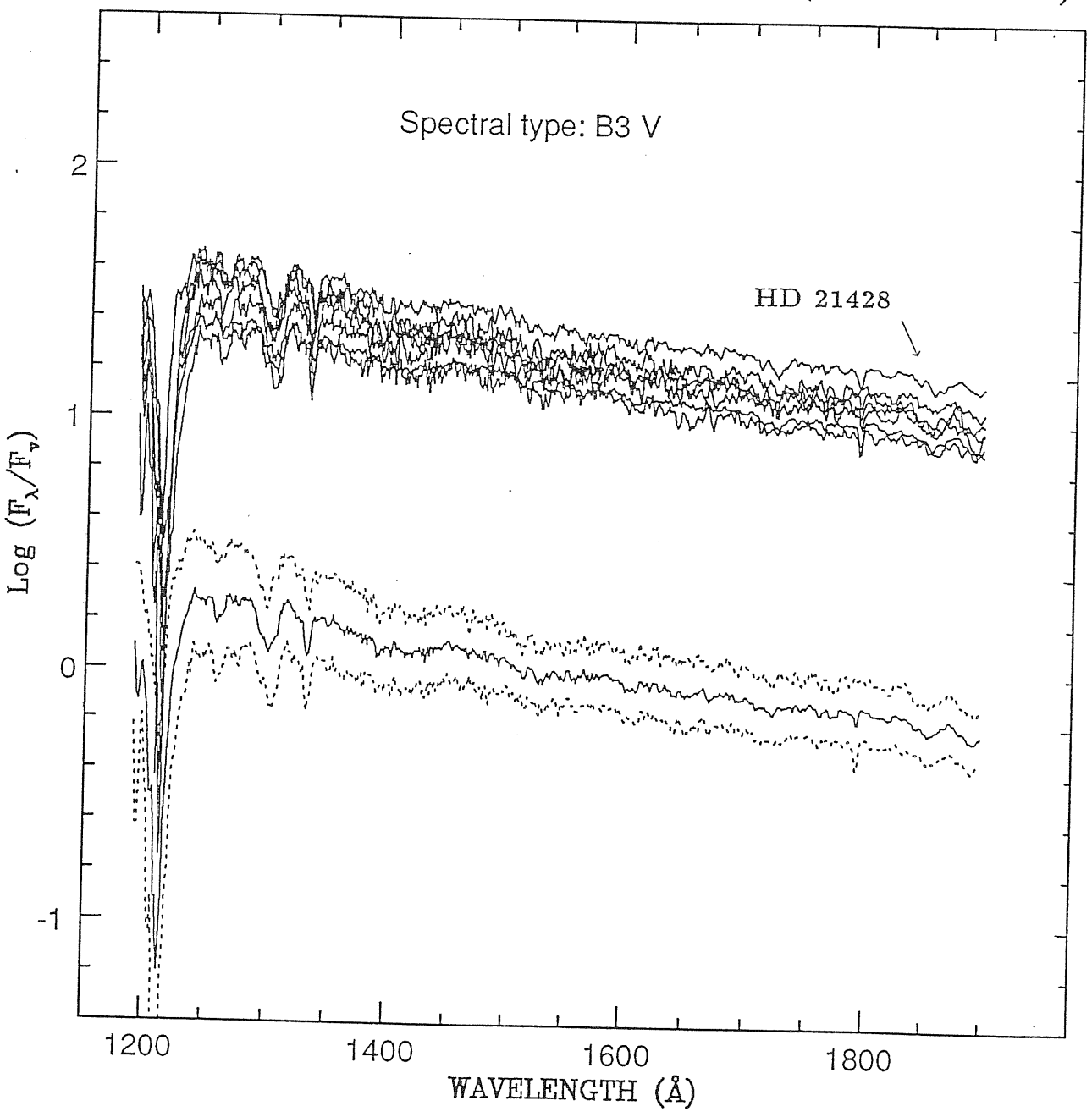

Fig. 2.1 (continued)

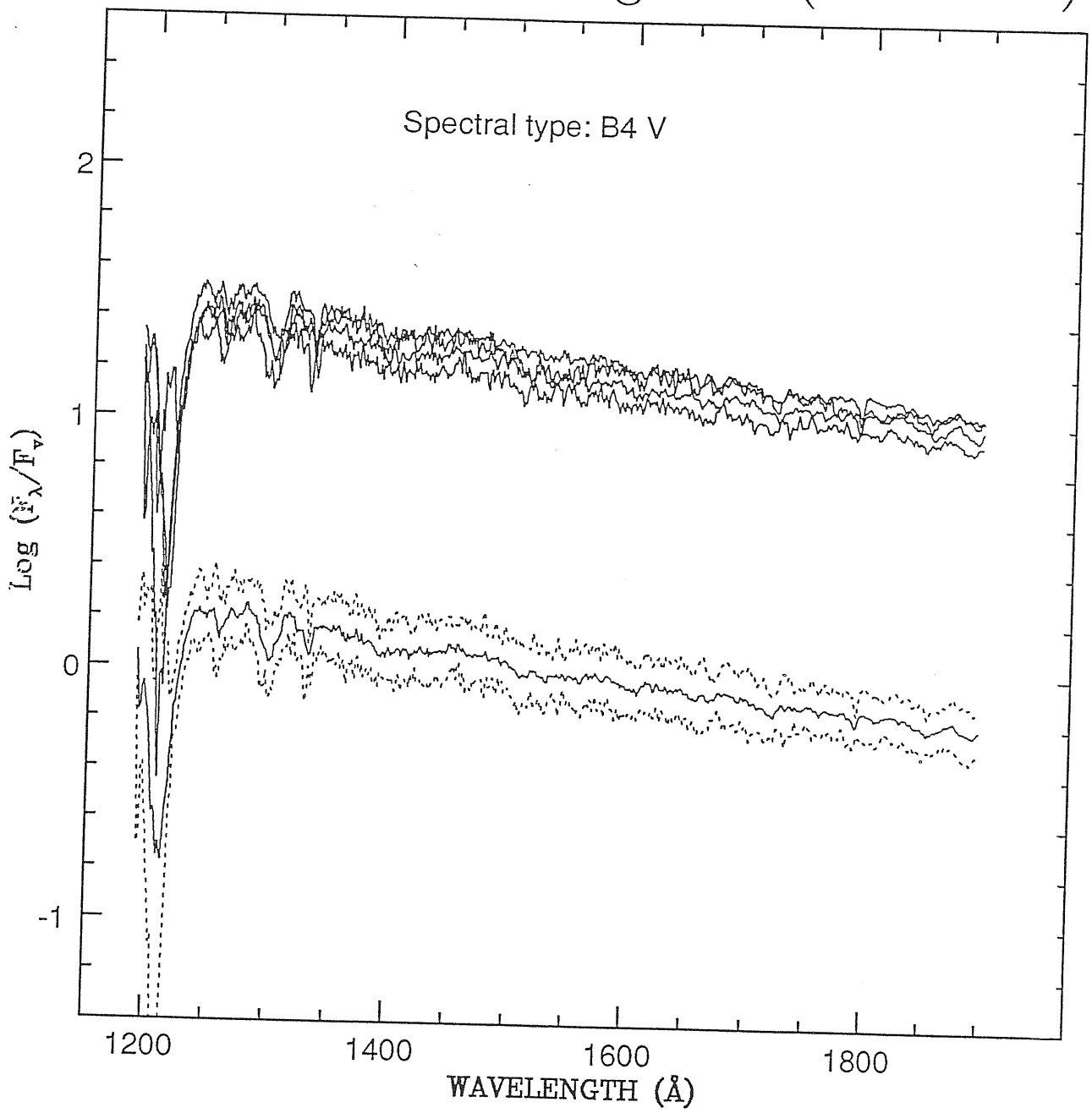

Fig. 2.1 (continued)

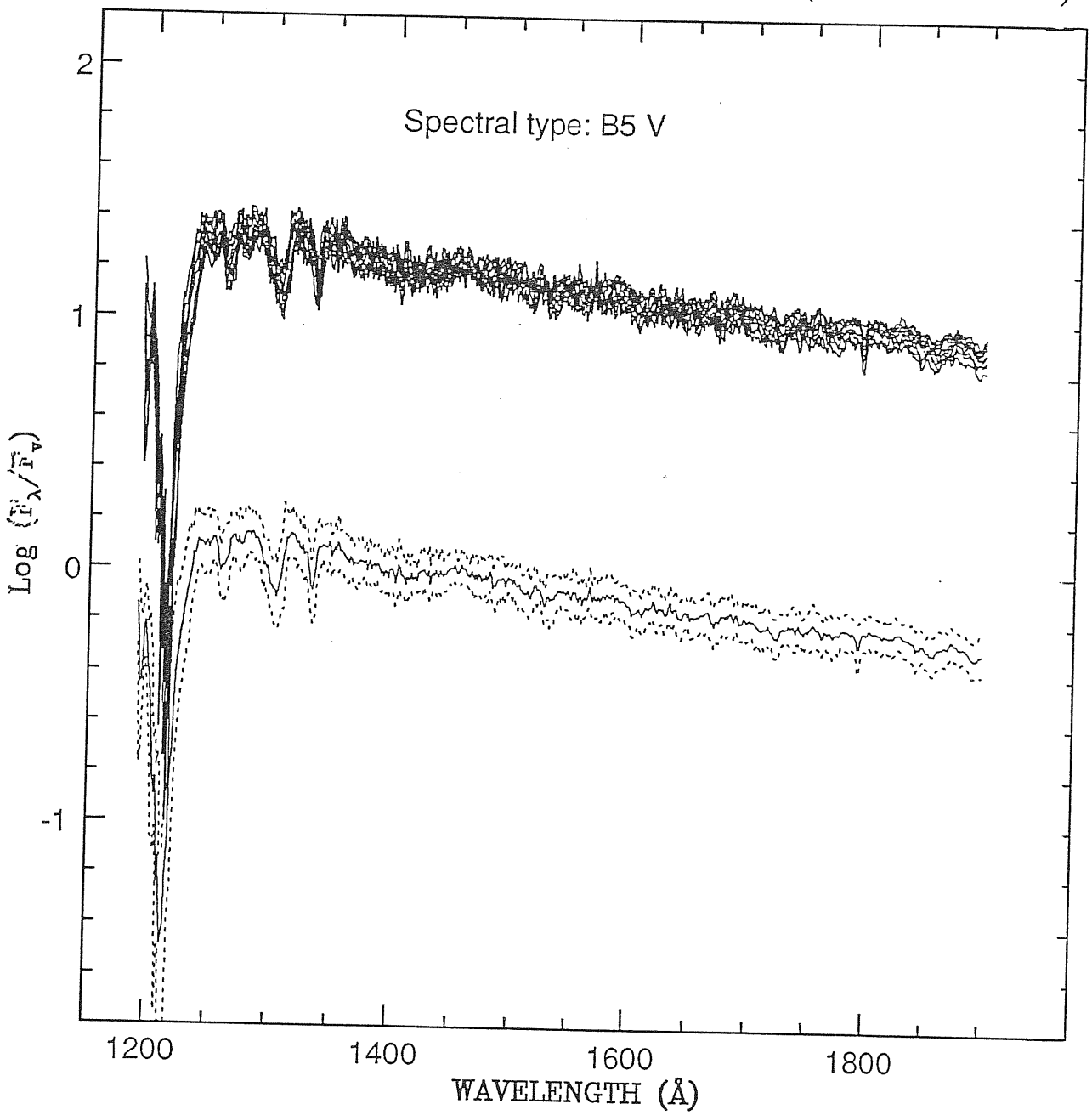

Fig. 2.1 (continued)

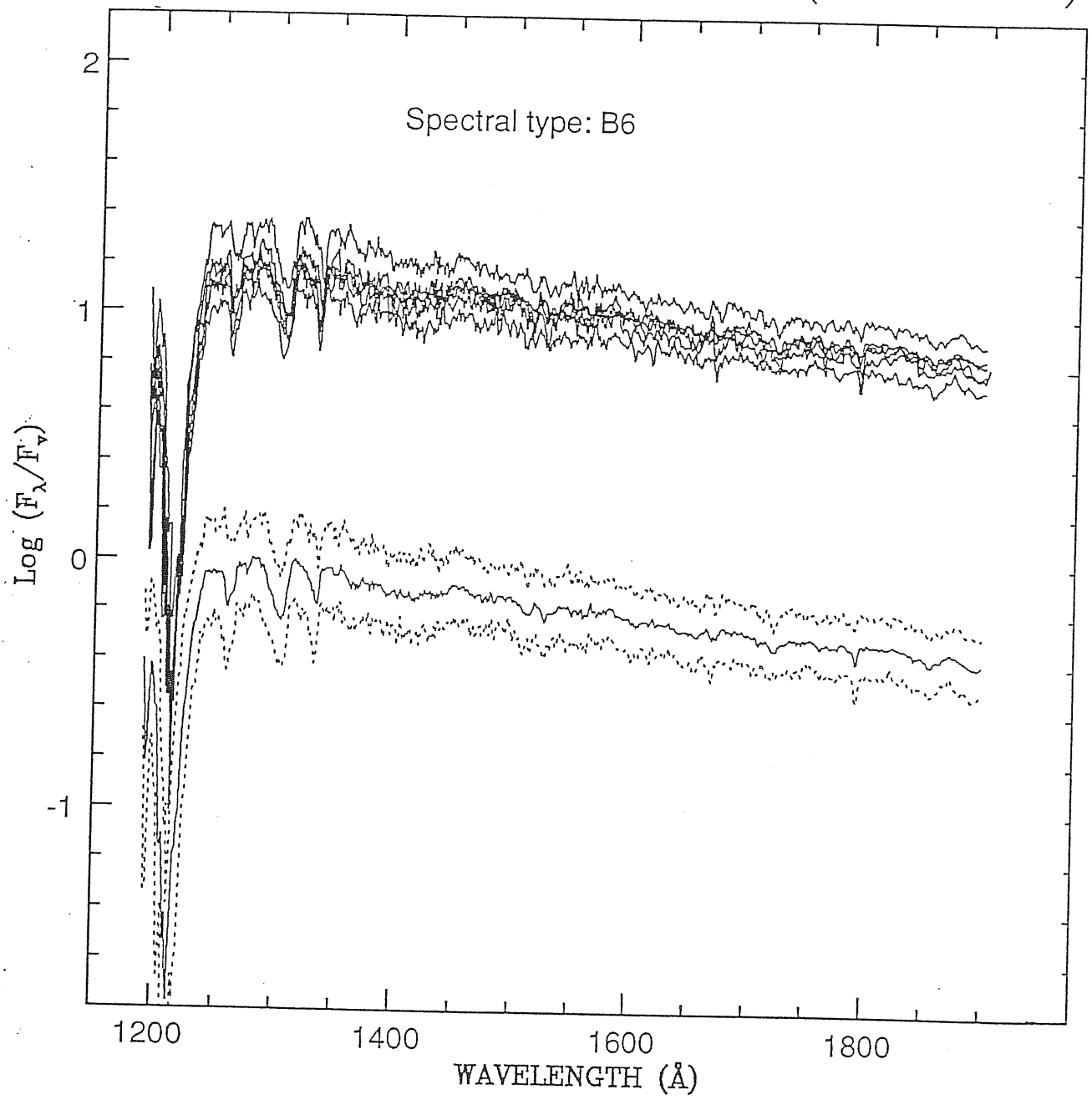

Fig. 2.1 (continued)

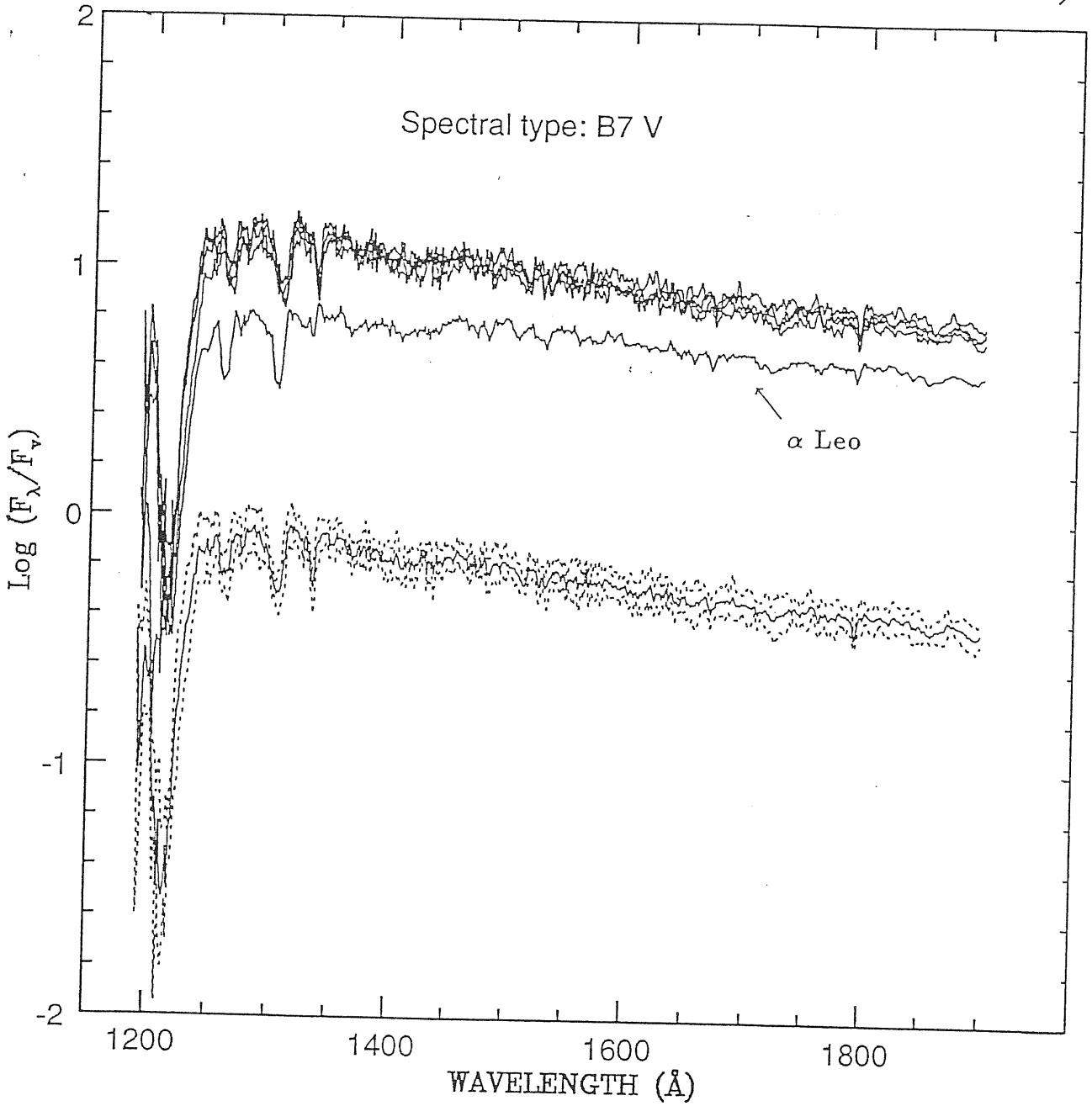

Fig. 2.1 (continued)

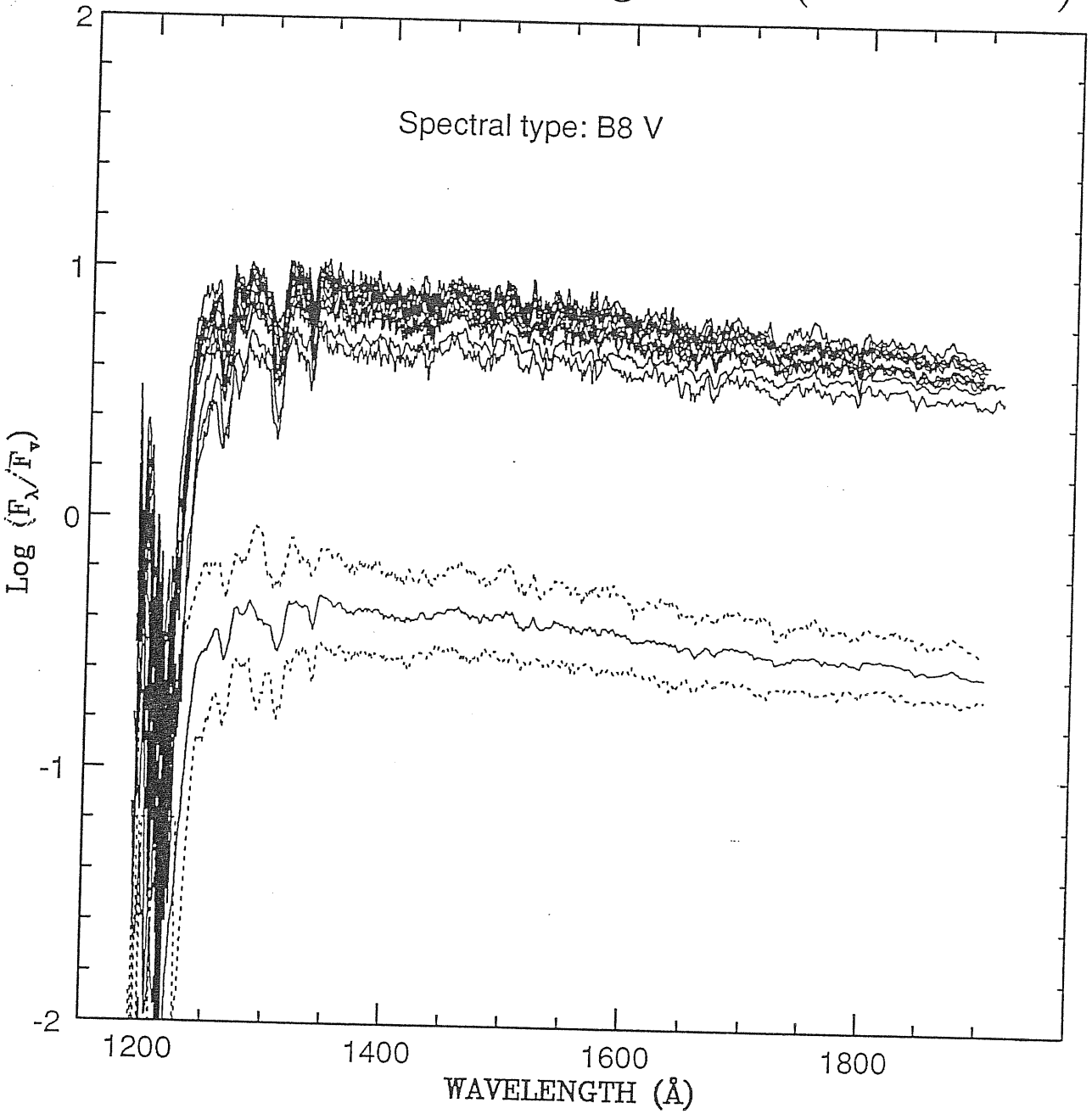

Fig. 2.1 (continued)

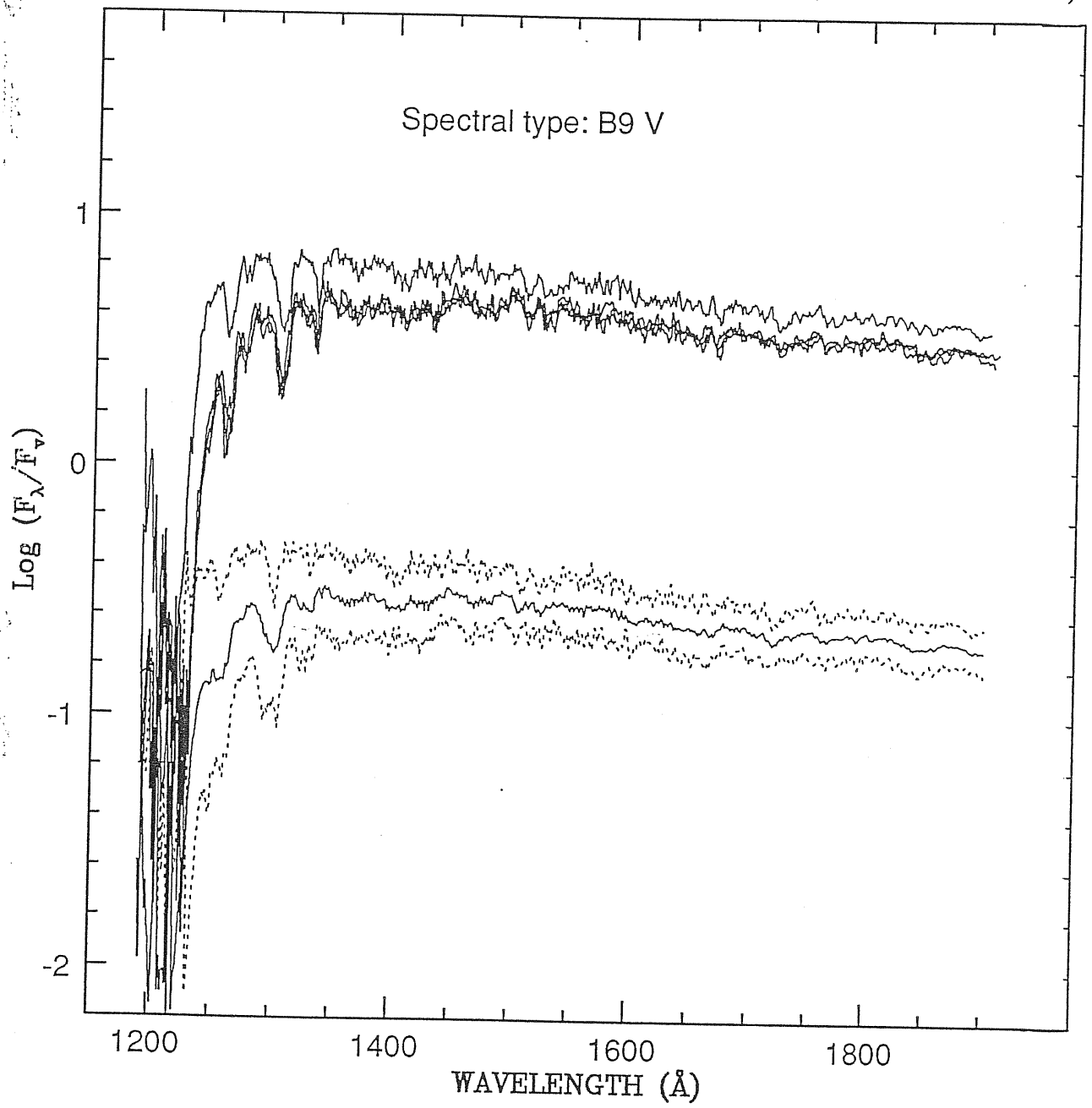

Fig. 2.2

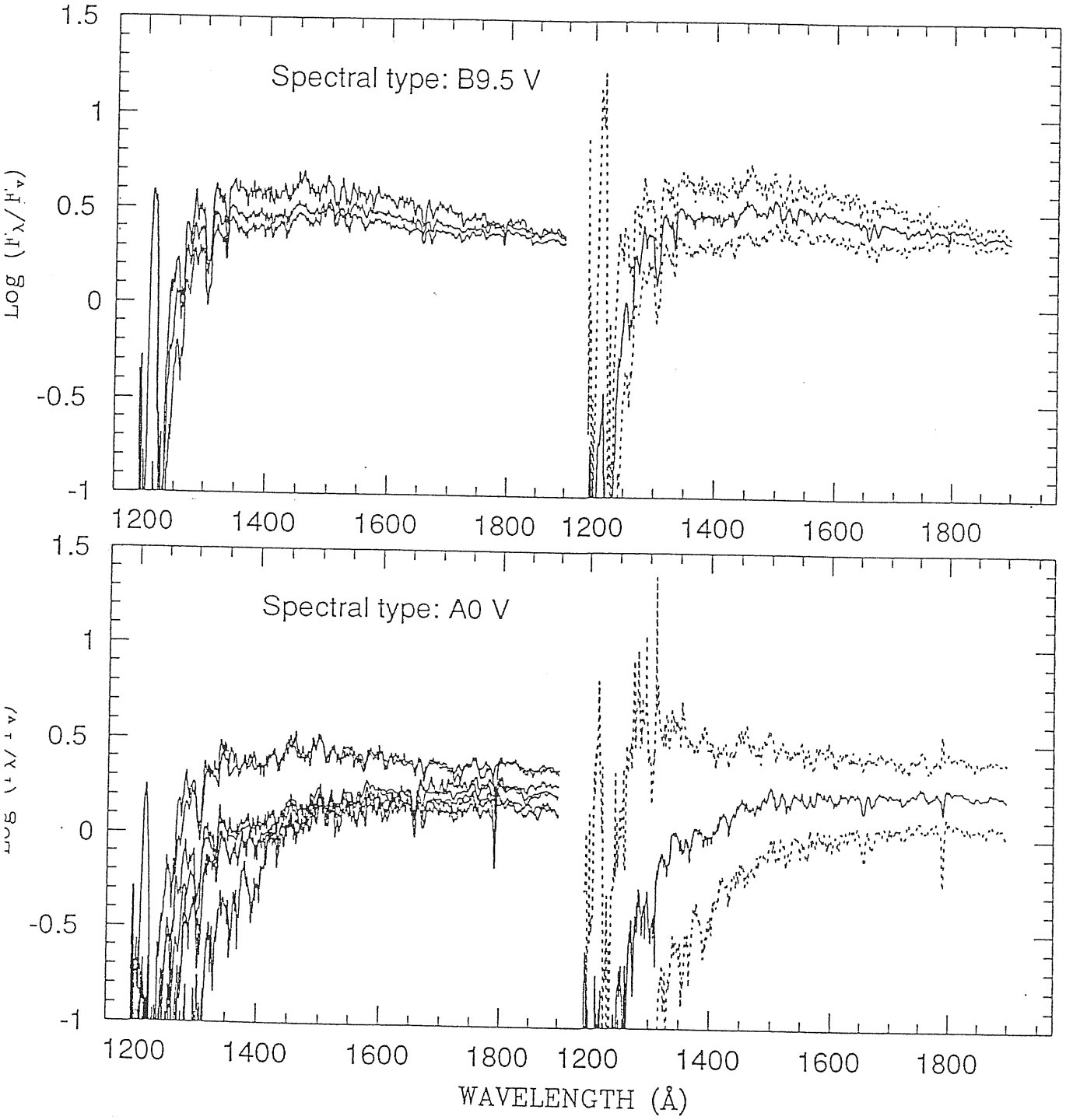
Spectral type: B9.5 V
Spectral type: A0 V
Log (Fλ/Fv)
1.5
1
0.5
0
-0.5
-1
1200
1400
1600
1800
WAVELENGTH (Å)

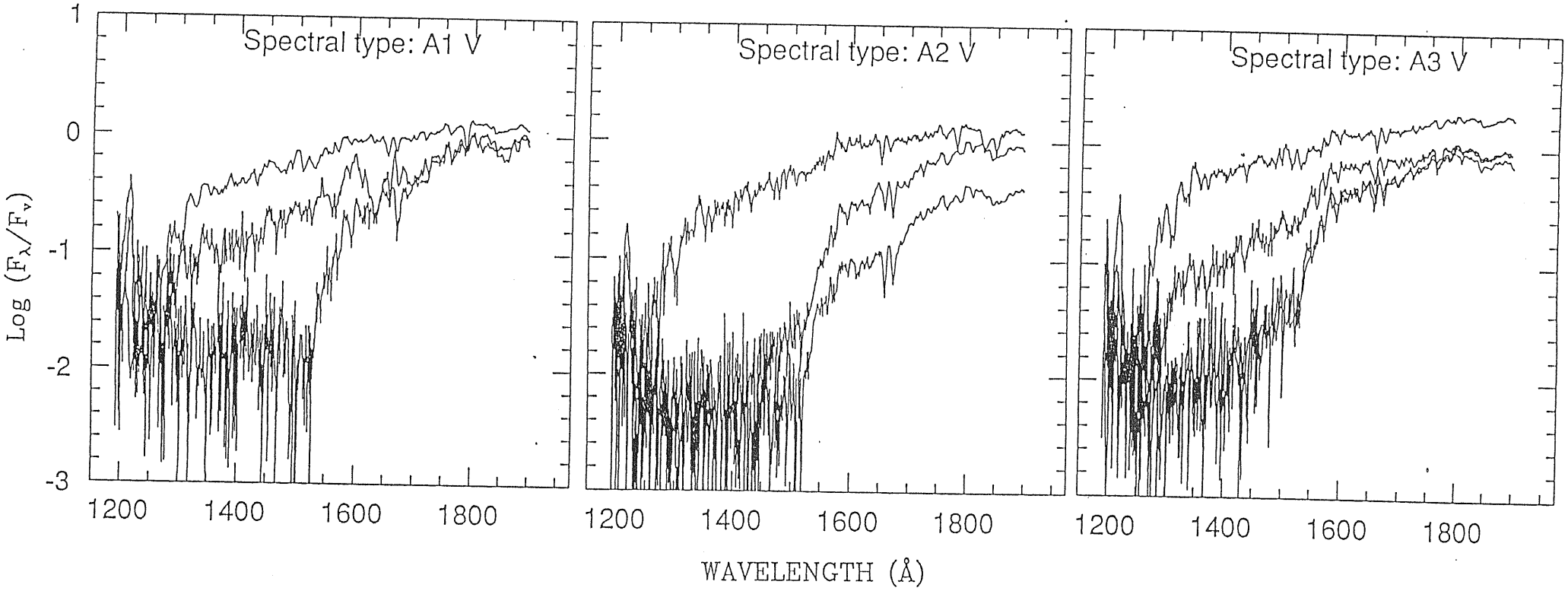
Spectral type: A1 V
Spectral type: A2 V
Spectral type: A3 V
Log (F_λ/F_v)
1
0
-1
-2
-3
1200
1400
1600
1800
WAVELENGTH (Å)

Fig. 2.3

Fig. 2.4 a

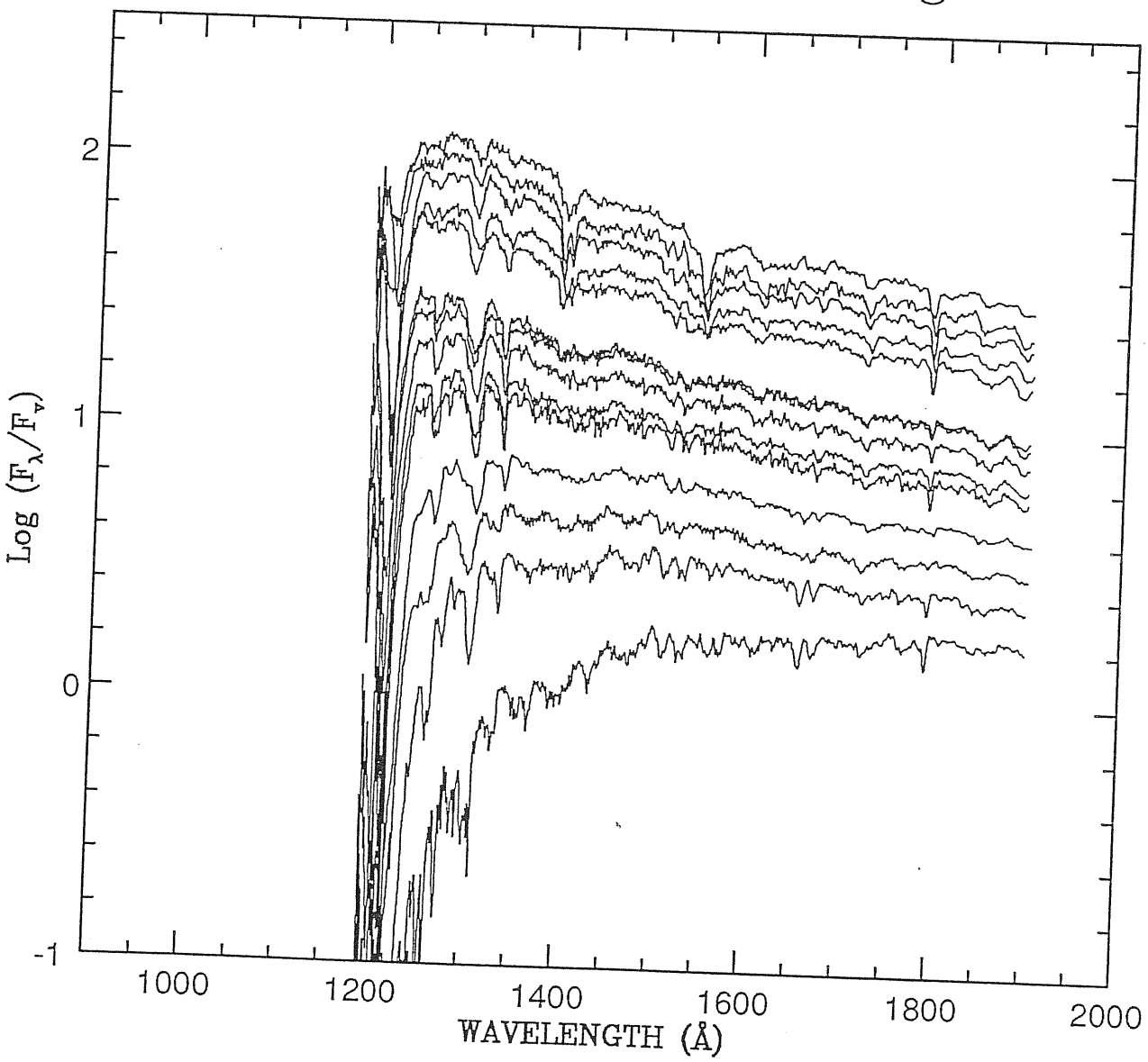
2
1
0
-1
Log (F_λ/F_ν)
1000
1200
1400
1600
1800
2000
WAVELENGTH (Å)

Fig. 2.4 b

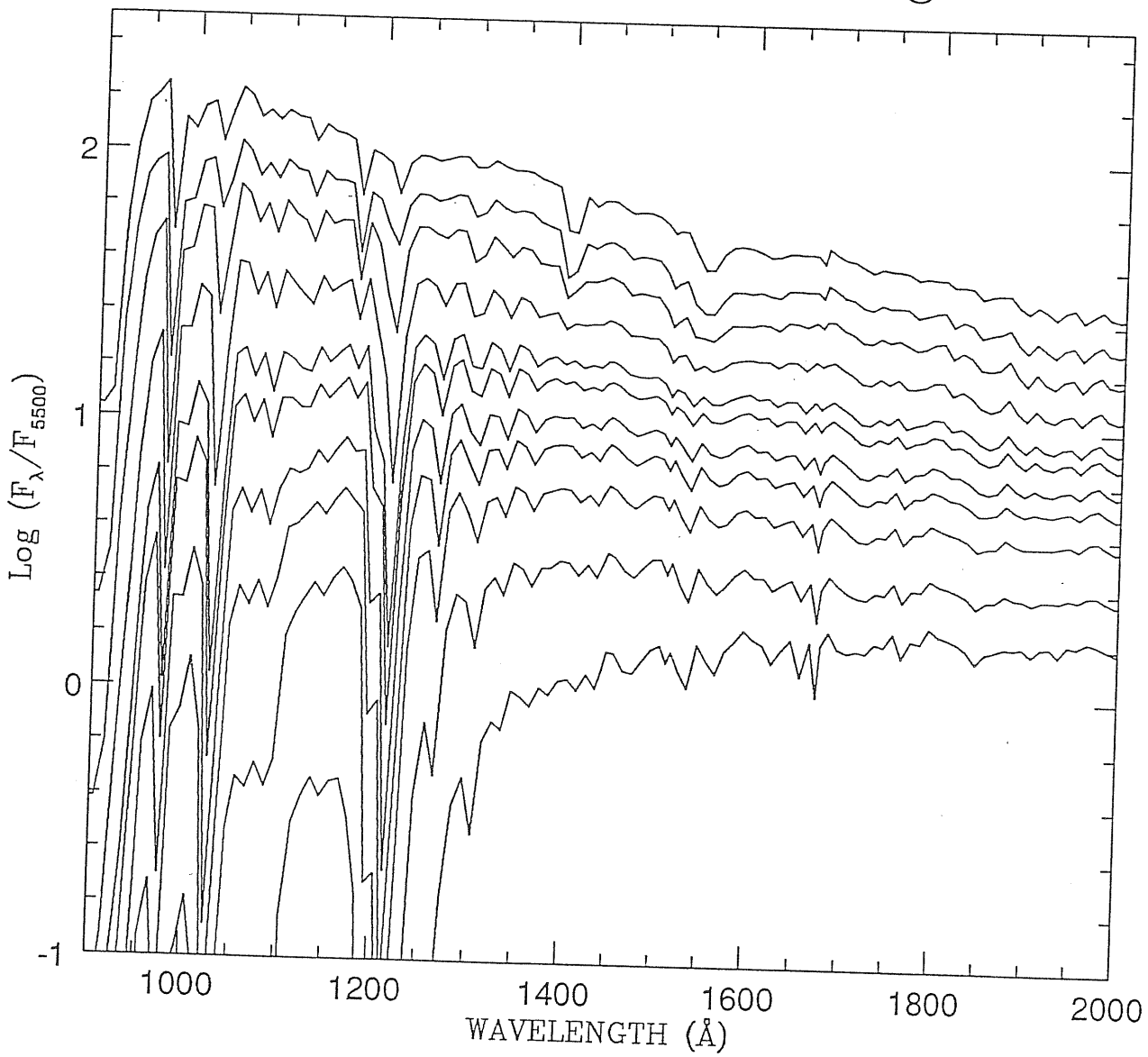
2
1
0
-1
Log (F_λ/F_{5500})
1000
1200
1400
1600
1800
2000
WAVELENGTH (Å)

Fig. 2.5

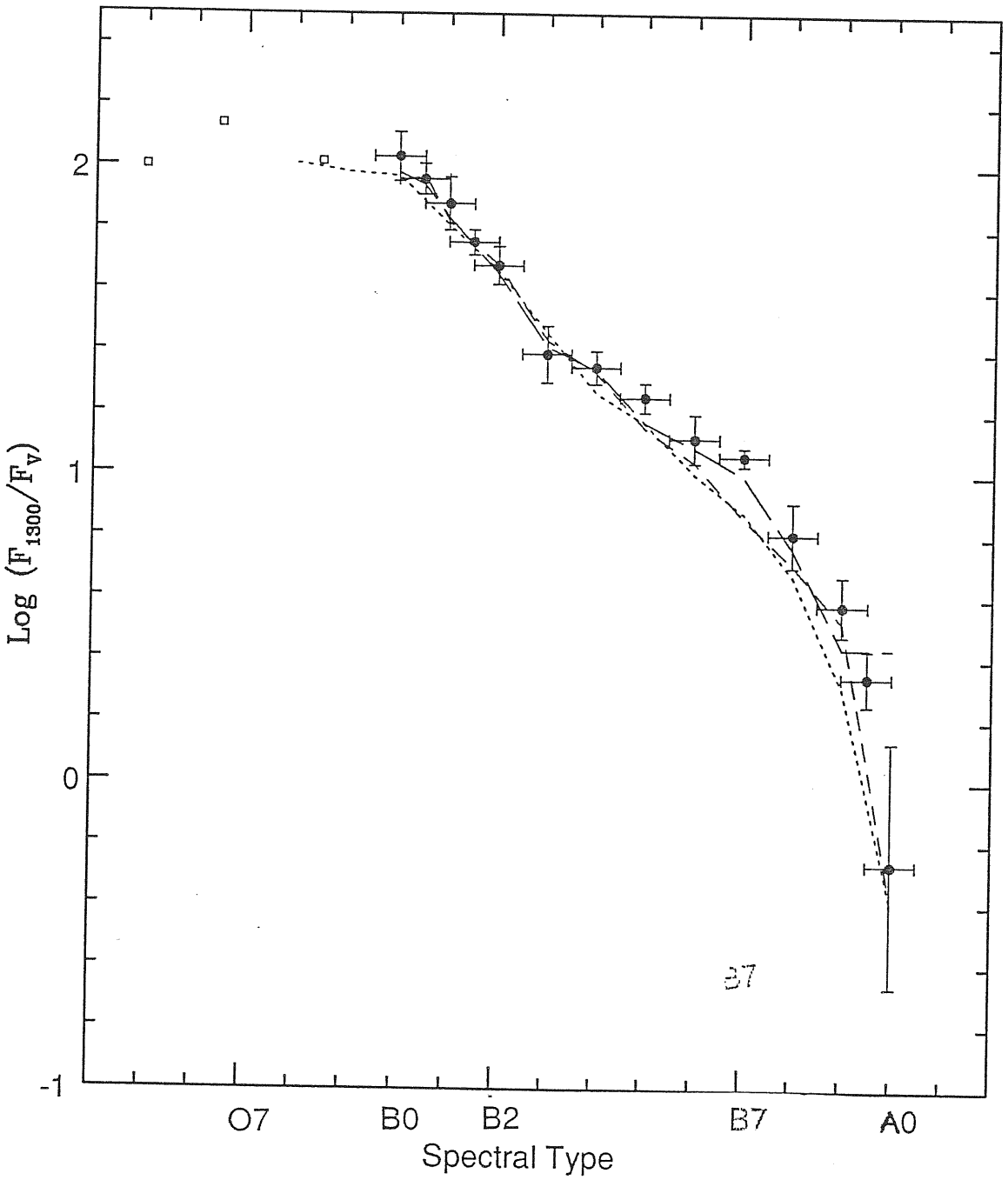

Fig. 2.5 (continued)

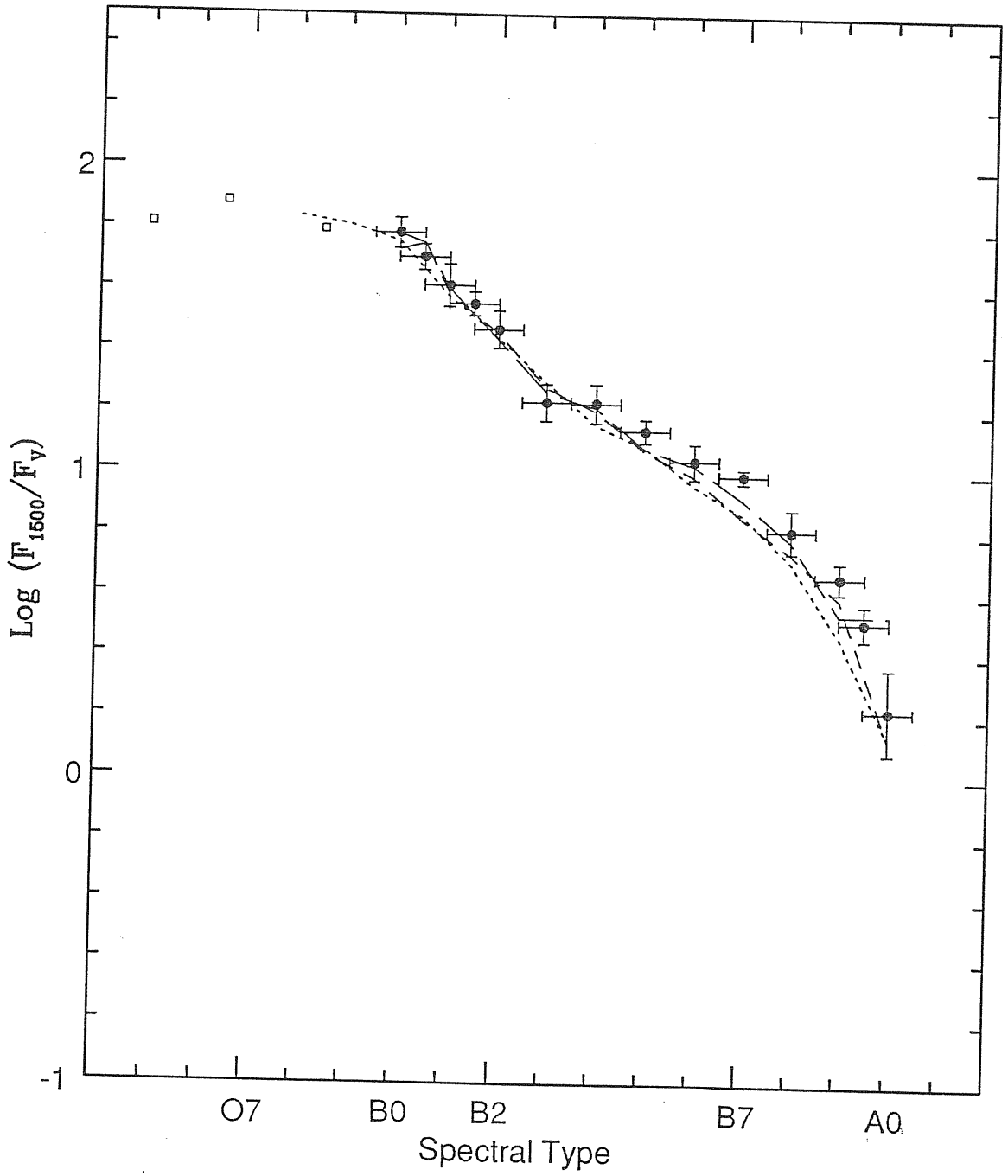

Fig. 2.5 (continued)

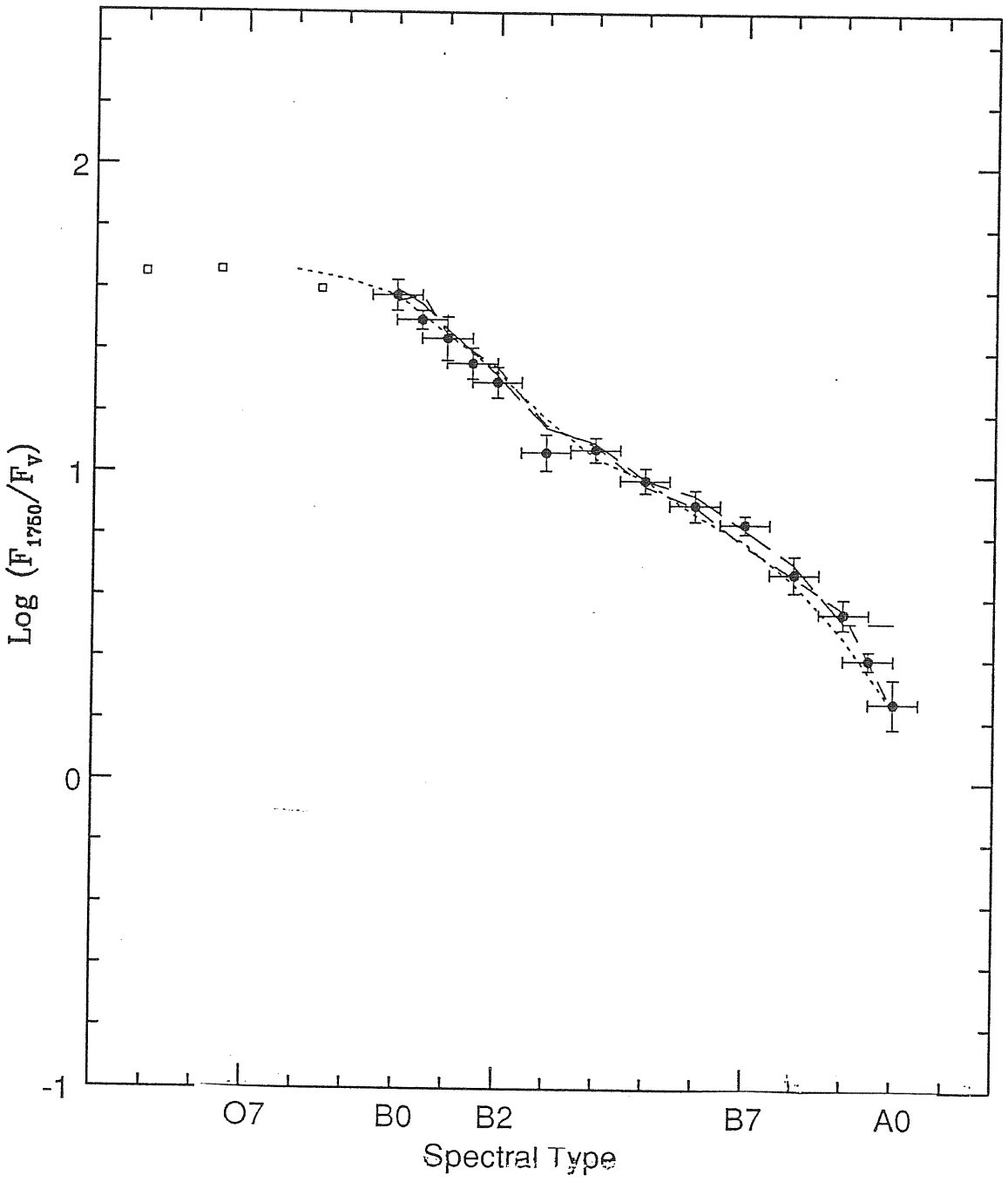

Fig. 2.6

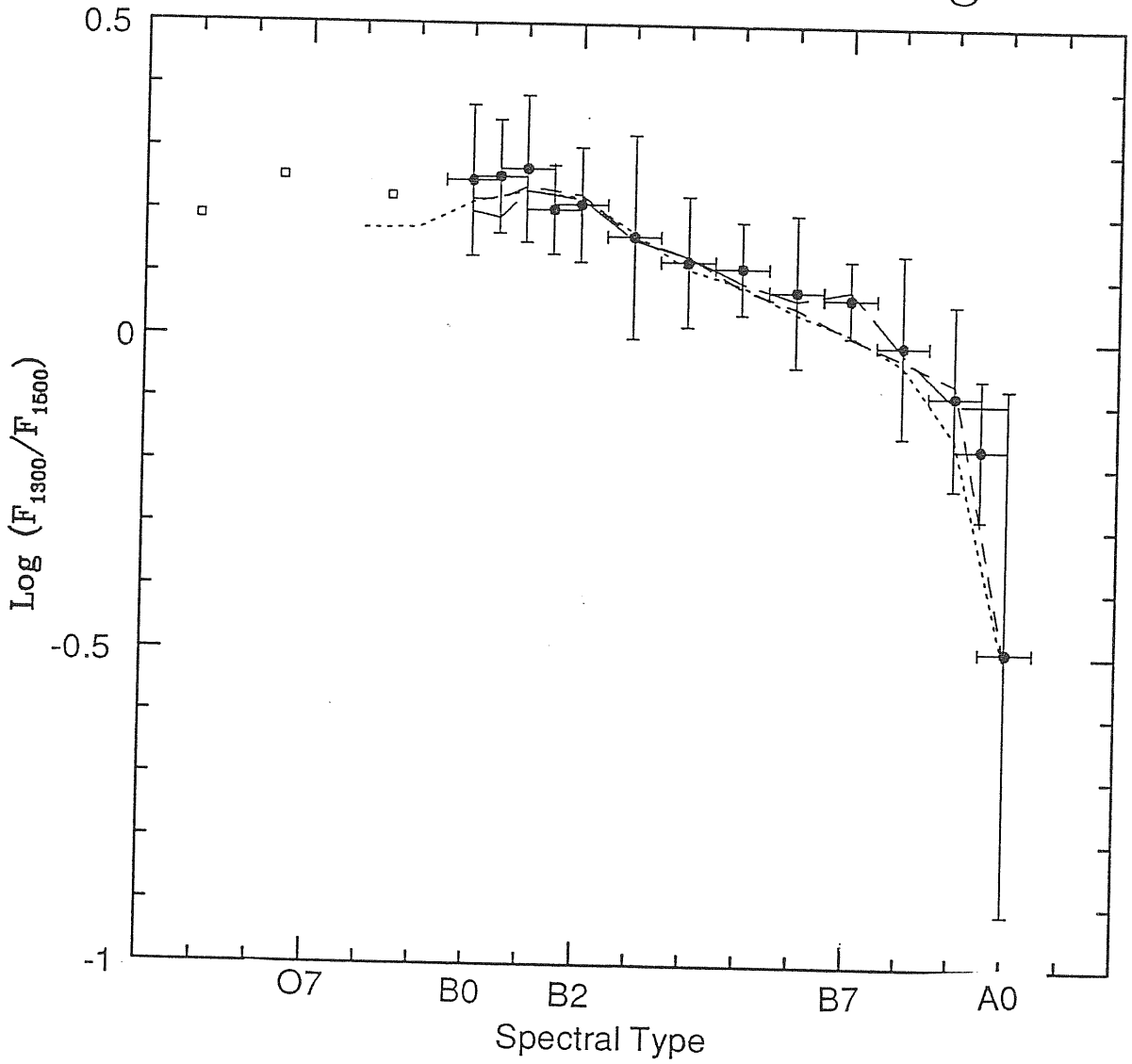

Fig. 2.6 (continued)

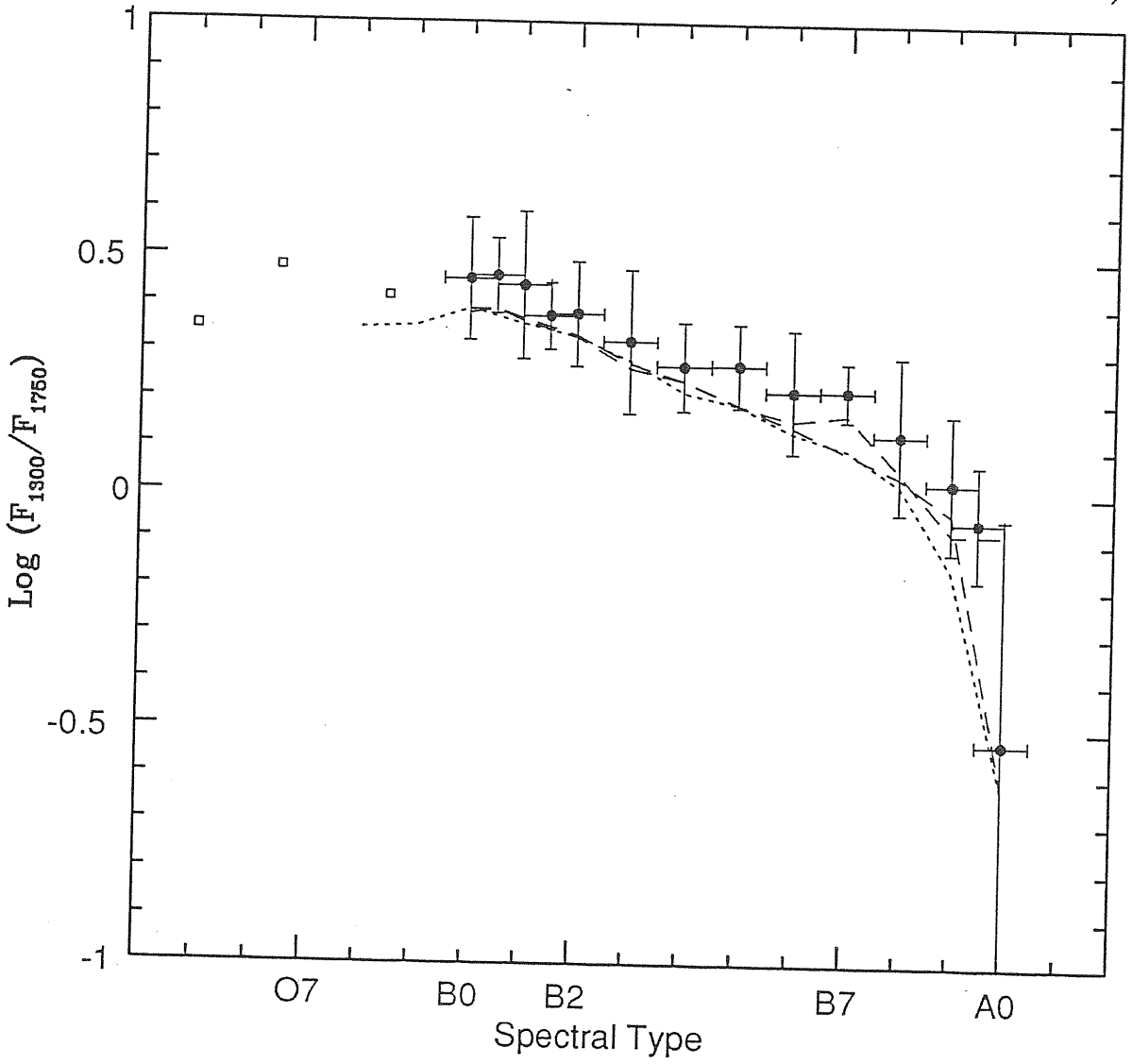

Fig. 3.1

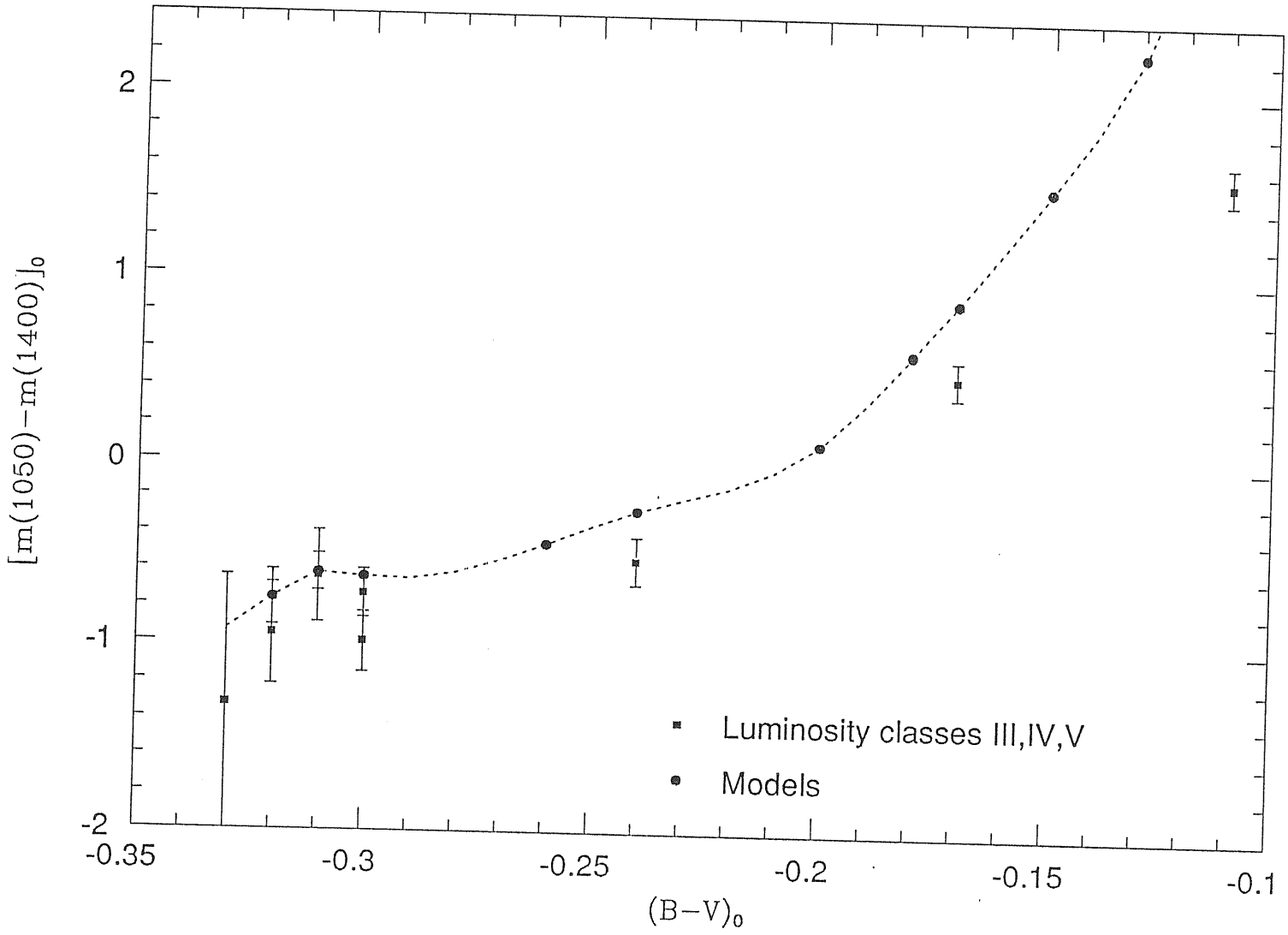
2
1
0
-1
-2
-0.35
-0.3
-0.25
-0.2
-0.15
-0.1
[m(1050)−m(1400)]₀
(B−V)₀
Luminosity classes III,IV,V
Models

Fig. 3.2

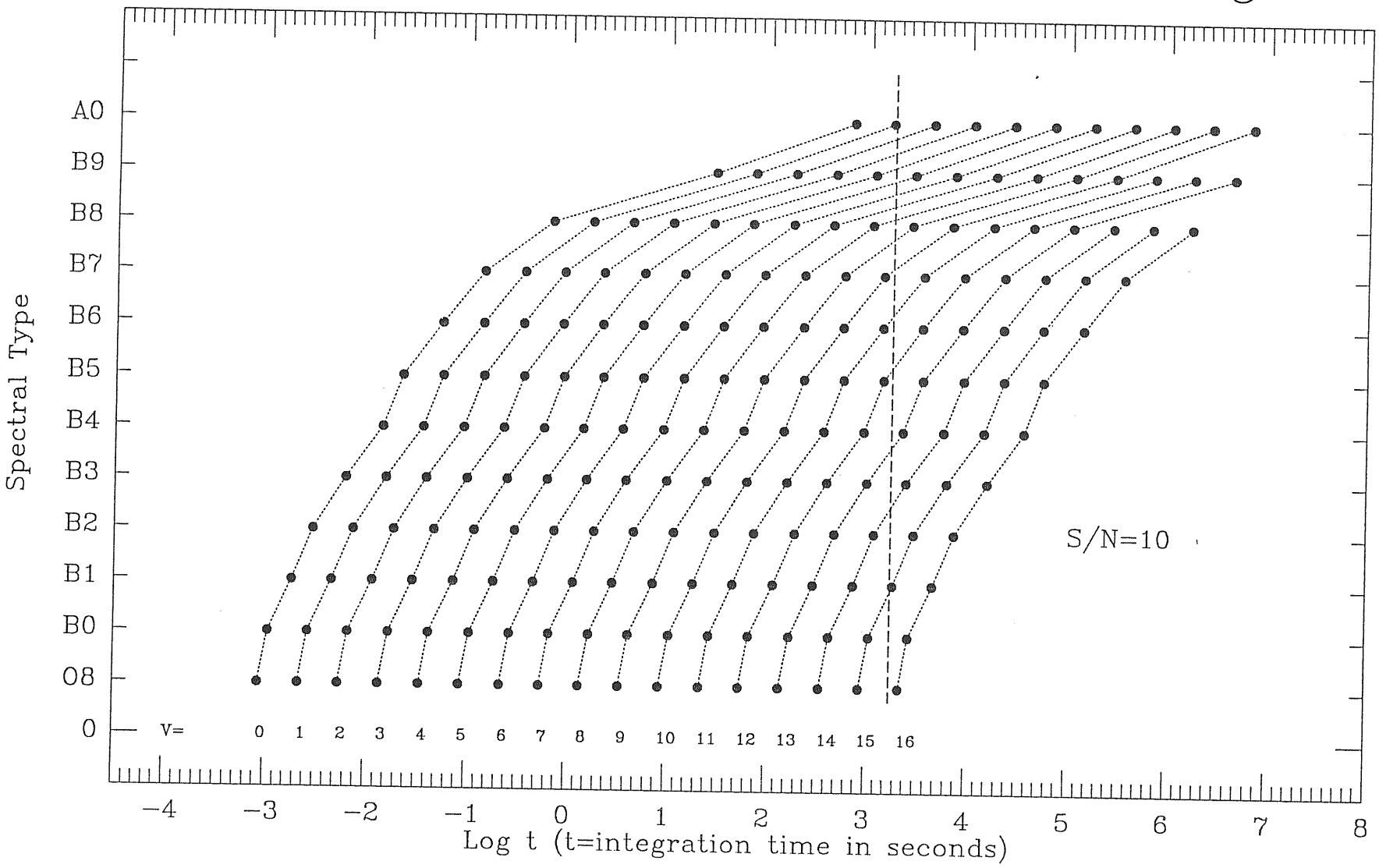
Spectral Type
A0
B9
B8
B7
B6
B5
B4
B3
B2
B1
B0
O8
O
V= 0 1 2 3 4 5 6 7 8 9 10 11 12 13 14 15 16
S/N=10
−4 −3 −2 −1 0 1 2 3 4 5 6 7 8
Log t (t=integration time in seconds)

Fig. 3.3

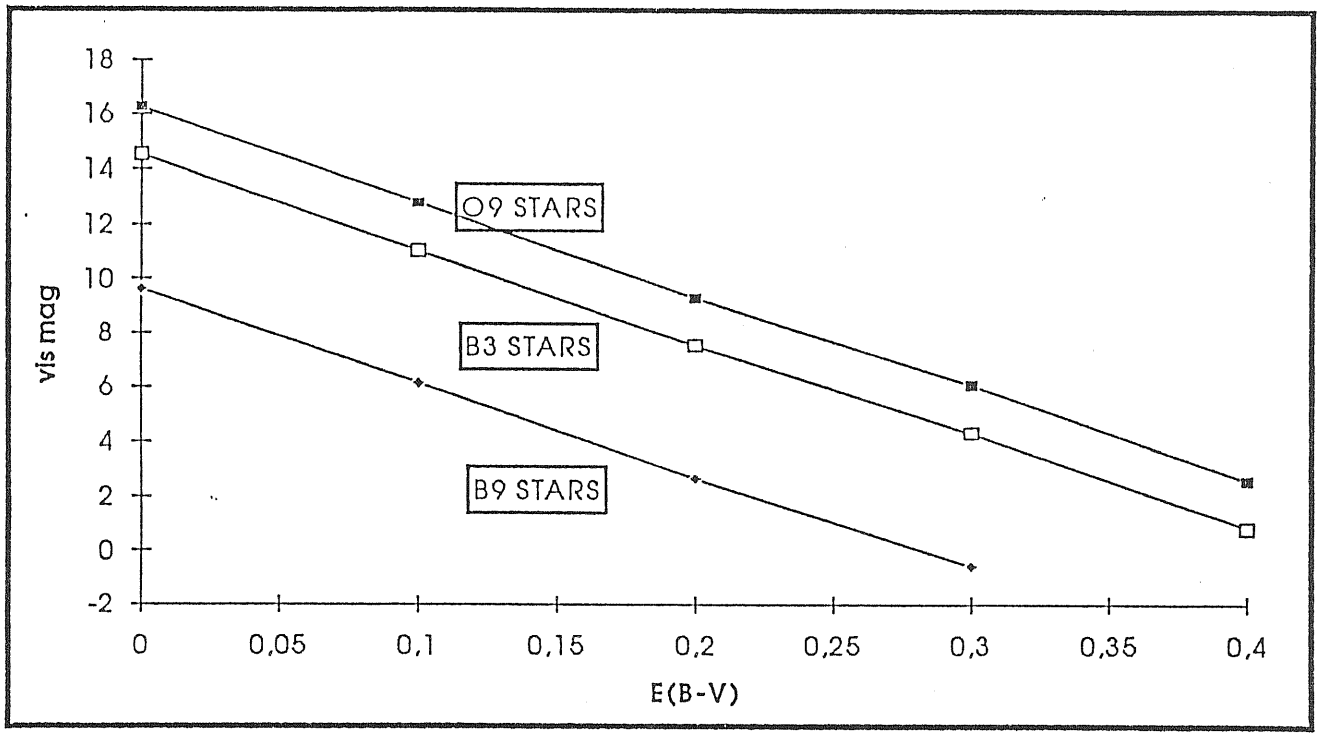
18
16
14
12
10
8
6
4
2
0
-2
vis mag
O9 STARS
B3 STARS
B9 STARS
0
0,05
0,1
0,15
0,2
0,25
0,3
0,35
0,4
E(B-V)

Tables

Table 1.1 Sensitivity parameters of UVSTAR.

λ	A	Ω	δ	σ	ε	μ	R	S
600	700	2.10^{-10}	.35	.11	.4	.35	3.7	.000017
1000	700	2.10^{-10}	.35	.15	.2	.45	3.3	.000015

Table 2.1: Program O Stars.

IMAGE	HD/BD	NAME	m_v	B-V	E(B-V)	ST
SWP 8696L	HD 164794	9 Sgr	5.97	+0.01	0.34	O4 ((f))[a]
SWP 8314L	HD 93205		7.8		0.37	O3 V[b]
SWP 8326L	HD 46223		7.27	+0.22	0.55	O5 e
SWP 8316L	HD 93250		7.4		0.48	O3 V((f))[b]
SWP 8313L	HD 93204		8.4		0.42	O5 V[b]
SWP 8697L	HD 168076		8.21	+0.47	0.80	O5
SWP 8315L	HD 303308		8.17		0.44	O3 V[b]
SWP33290L	HD 164492		7.63	+0.02	0.35	O6
SWP16112L	HD 151515		7.16	+0.17	0.49	O7 II...
SWP 6909L	HD 46150		6.75	+0.13	0.46	O6e
SWP23767L	HD 99897		8.36	+0.16	0.49	O6
SWP23769L	HD 101190		7.27	+0.06	0.38	O7
SWP 2861L	HD 54662		6.21	+0.03	0.35	O6.5 V[c]
SWP22768L	HD 38666	μ Col	5.20	-0.28	0.03	O9.5 V
SWP25946L	HD 214680	10 Lac	4.90	-0.20	0.11	O9 V
SWP 6910L	HD 46149		7.59	+0.17	0.49	O8.5 V
SWP 8150L	HD 14633		7.47	-0.21	0.11	O8.5 V
SWP18252L	HD 149757	ζ Oph	2.60	+0.02	0.33	O9 V
SWP15683L	HD 34078	AE Aur	5.94	+0.22	0.53	O9.5 Ve var
SWP22813L	HD 60848		6.85	-0.21	0.11	O8 Vpevar
SWP16225L	HD 93521		7.06	-0.28	0.03	O9 Vp

[a] The spectral type adopted is from Conti and Leep (1974).
[b] For these stars the spectral type and color excess are from Herbst (1976).
[c] Spectral type from Walborn (1973).

Table 2.2: Program B stars

IMAGE	HD/BD	NAME	m_v	B-V	E(B-V)	ST	remarks
SWP17530L	BD+56 501		9.45	+0.26	0.56	B0 V	
SWP13451L	HD 239729		8.35	+0.36	0.66	B0 V	
SWP11155L	HD 36512	υ Ori	4.62	-0.263	0.037	B0 V	
SWP33008L	HD 149438	τ Sco	2.82	-0.25	0.06	B0 V	
SWP23117L	HD 55857		6.10	-0.22	0.06	B0.5 V	v
SWP16572L	HD 211880		7.75	+0.32	0.60	B0.5 V	*
SWP30227L	HD 36960		4.78	-0.25	0.03	B0.5 V	
SWP15680L	HD 38131		8.19	+0.21	0.49	B0.5 V	
SWP25376L	HD 210832		7.50	-0.20	0.08	B0.5 V	
SWP24120L	HD 326333		9.65	+0.20	0.46	B1 V	v
SWP28199L	HD 46660		8.04	+0.31	0.57	B1 V	
SWP19382L	CD-41 11032		9.43	+0.16	0.42	B1 V	
SWP29155L	HD 208440		7.90	+0.07	0.33	B1 V	
SWP11140L	HD 154445		5.64	+0.16	0.42	B1 V	
SWP13448L	HD 46106		7.92	+0.14	0.40	B1 V	
SWP34153L	BD+52 3210		10.69	-0.02	0.24	B1 V	
SWP33202L	HD 166197		6.15	-0.16	0.10	B1 V	v
SWP17531L	BD+56 517		10.50	+0.27	0.52	B1.5 V	
SWP24133L	BD-13 4920		10.06	+0.48	0.73	B1.5 V	*
SWP24118L	HD 326328		10.23	+0.22	0.47	B1.5 V	*
SWP24962L	HD 74273		5.90	-0.21	0.04	B1.5 V	
SWP32568L	HD 64740		4.60	-0.24	0.01	B1.5 Vp	
SWP19437L	HD 37017		6.56	-0.13	0.12	B1.5 V	
SWP24121L	HD 152560		8.27	+0.12	0.36	B2 V	*
SWP32877L	HD 142669	ρ Sco	3.90	-0.19	0.05	B2 IV-V	
SWP14308L	HD 64802		5.50	-0.18	0.06	B2 V:n	
SWP32569L	HD 54669		6.65	-0.21	0.03	B2 V	
SWP19500L	HD 32612		8.78	-0.17	0.07	B2 IV	
SWP16395L	HD 37776		6.98	-0.15	0.09	B2 IV	v
SWP25372L	HD 32630	η Aur	3.20	-0.18	0.02	B3 V	v
SWP27577L	HD 36954		6.94	-0.11	0.09	B3 V	
SWP31546L	HD 20365	29 Per	5.15	-0.06	0.14	B3 V	
SWP29648L	HD 37526		7.55	-0.14	0.06	B3 V	
SWP30190L	HD 45725	β Mon A	4.60	-0.10	0.10	B3 Ve	
SWP26251L	HD 120315	η UMa	1.86	-0.191	0.009	B3 V	v
SWP14768L	HD 21428	34 Per	4.67	-0.09	0.11	B3 V	*
SWP30023L	HD 38023		8.86	+0.31	0.49	B4 V	
SWP15557L	HD 65904		5.99	-0.14	0.04	B4 V	
SWP23719L	HD 136664		4.54	-0.15	0.03	B4 V	
SWP14611L	HD 4142		5.68	-0.13	0.05	B4 V	
SWP27598L	HD 37272		7.91	-0.12	0.05	B5 V	
SWP26272L	HD 106911	β Cha	4.30	-0.13	0.04	B5 Vn	v
SWP27578L	HD 37525		8.08	-0.09	0.08	B5 V	
SWP27588L	HD 37332		7.60	-0.14	0.03	B5 V	
SWP27596L	HD 36826		8.21	+0.00	0.17	B5 Vn	

Table 2.2: Program B stars (*Continued*)

IMAGE	HD/BD	NAME	m_v	B-V	E(B-V)	ST	remarks
SWP29295L	HD 36936		7.57	-0.12	0.05	B5 V	
SWP29247L	HD 36151		6.71	-0.11	0.06	B5 V	
SWP31602L	HD 20418		5.02	-0.06	0.11	B5 V	
SWP31603L	HD 20809		5.30	-0.08	0.09	B5 V	
SWP29248L	HD 36487		7.81	-0.11	0.06	B5 V	
SWP22742L	HD 182918		8.61	+0.15	0.30	B6 V	*
SWP27589L	HD 37112		8.02	-0.09	0.06	B6 V	
SWP31556L	HD 24504		5.38	-0.08	0.07	B6 V	
SWP29294L	HD 37700		7.90	-0.11	0.04	B6 V	
SWP29649L	HD 38755		7.62	-0.11	0.04	B6 V	
SWP15791L	HD 90994	β Sex	5.09	-0.14	0.01	B6 V	
SWP27597L	HD 37173		7.86	-0.06	0.09	B6 V	
SWP27599L	HD 37641		7.56	-0.06	0.07	B7 V	
SWP27616L	HD 36760		7.64	-0.10	0.03	B7 V	
SWP32307L	HD 87901	α Leo	1.35	-0.11	0.02	B7 V	*
SWP29650L	HD 36842		8.13	-0.09	0.04	B7 V	
SWP27617L	HD 36935		7.50	-0.13	0.00	B7 V	
SWP25009L	HD 74604		6.20	-0.11	0.00	B8 V	
SWP26270L	HD 214923	ζ Peg	3.40	-0.08	0.03	B8 V	
SWP25663L	HD 158094	δ Ara	3.60	-0.10	0.01	B8 Vn	
SWP27623L	HD 37151		7.38	-0.08	0.03	B8 V	v
SWP27587L	HD 37235		8.17	-0.10	0.01	B8 V	
SWP31560L	HD 22136		6.89	-0.01	0.10	B8 V	
SWP31561L	HD 21672		6.63	-0.02	0.09	B8 V	
SWP31593L	HD 23923		6.17	-0.05	0.06	B8 V	
SWP31599L	HD 23432	21 Tau	5.80	-0.04	0.07	B8 V	v
SWP29249L	HD 36541		7.69	-0.10	0.01	B8 V	
SWP29443L	HD 23324	18 Tau	5.64	-0.07	0.04	B8 V	
SWP33362L	HD 201908		5.92	-0.07	0.04	B8 Vn	
SWP26194L	HD 16978	ϵ Hyi	4.11	-0.06	0.01	B9 V	
SWP27593L	HD 36915		8.01	-0.01	0.06	B9 V	
SWP27595L	HD 36628		7.98	-0.04	0.03	B9 V	
SWP31558L	HD 21931		7.34	+0.04	0.11	B9 V	
SWP18885L	HD 108767	δ Crv	2.95	-0.04	0.005	B9.5 V	
SWP26036L	BD+69 1231		9.28	+0.14	0.185	B9.5 V	
SWP26193L	HD 212581	δ Tuc	4.50	-0.03	0.015	B9.5 V	

Remarks: An asterisk means that the star was not used in the average. v stands for variable or suspected variables according to SIMBAD.

Table 2.3: Program A stars

IMAGE	HD/BD	NAME	m_v	B-V	E(B-V)	ST
SWP19125L	HD 110411	ρ Vir	4.88	+0.08	0.10	A0 V
SWP31549L	HD 130109		3.72	+0.00	0.02	A0 V
SWP11257L	HD 62001		8.18	+0.055	0.075	A0 V
SWP29459L	HD 23964		6.74	+0.06	0.08	A0 V
SWP 6475L	HD 9132		5.12	+0.02	0.04	A0 V
SWP 5769L	HD 38206		5.73	-0.01	0.01	A0 V
SWP 8198L	HD 103287	γ Uma	2.44	+0.00	0.02	A0 V
SWP20736L	HD 6619		6.61	+0.14	0.13	A1 V
SWP28839L	HD 163296		6.85	+0.07	0.06	A1 V
SWP9282L	HD 65810		4.60	+0.08	0.07	A1 V
SWP20732L	HD 40932		4.13	+0.16	0.11	A2 V
SWP16301L	HD 48097		5.21	0.06	0.01	A2 V
SWP 4959L	HD 39283		5.00	+0.05	0.00	A2 V
SWP20734L	HD 11031		5.82	+0.29	0.21	A3 V
SWP31145L	HD 102647	β Leo	2.14	+0.08	0.00	A3 V
SWP30306L	HD 16970	γ Cet	3.47	+0.09	0.01	A3 V
SWP 9134L	HD 216956	α PsA	1.16	+0.09	0.01	A3 V

Table 2.4: Mean observed fluxes and model predictions

ST	T_{eff}	F_{13}^M	F_{13}	σ_{13}	F_{15}^M	F_{15}	σ_{15}	F_{17}^M	F_{17}	σ_{17}
O5	48200		1.99	0.06		1.81	0.04		1.65	0.04
O6-O7	40000		2.13	0.08		1.88	0.06		1.66	0.05
O8-O9	34200	2.01/1.98[a]	2.01	0.08	1.84/1.80[a]	1.79	0.08	1.66/1.63[a]	1.60	0.06
B0	30000	1.97	2.03	0.05	1.75	1.78	0.05	1.58	1.58	0.05
B0.5	27700		1.96	0.05		1.70	0.04		1.50	0.03
B1	25400	1.81	1.88	0.08	1.57	1.61	0.07	1.45	1.44	0.07
B1.5	23700		1.76	0.04		1.55	0.04		1.38	0.03
B2	22000	1.66	1.68	0.06	1.44	1.46	0.06	1.33	1.30	0.05
B3	18700	1.46	1.39	0.09	1.29	1.23	0.06	1.18	1.07	0.06
B4	16300	1.26	1.35	0.05	1.15	1.22	0.06	1.05	1.08	0.04
B5	15400	1.17	1.25	0.04	1.08	1.14	0.04	0.98	0.98	0.04
B6	14000	1.00	1.11	0.08	0.96	1.04	0.06	0.87	0.90	0.05
B7	13000	0.87	1.06	0.03	0.86	0.99	0.03	0.78	0.84	0.03
B8	11900	0.67	0.80	0.10	0.71	0.81	0.07	0.65	0.68	0.06
B9	10500	0.31	0.57	0.09	0.47	0.66	0.05	0.47	0.55	0.05
B9.5	10000		0.34	0.09		0.52	0.06		0.40	0.03
A0	9520	-0.38	-0.26	0.39	0.13	0.23	0.14	0.24	0.26	0.08

[a] These values correspond to the computed fluxes for O8 and O9 stars separatedly